Journal of Experimental Botany, Vol. 73, No. 5 pp. 1327–1343, 2022
https://doi.org/10.1093/jxb/erab504 Advance Access Publication 19 November 2021

RESEARCH PAPER

Lysophosphatidic acid acyltransferases: a link with intracellular protein trafficking in Arabidopsis root cells?

Valérie Wattelet-Boyer[1], Marina Le Guédard[1,2], Franziska Dittrich-Domergue[1], Lilly Maneta-Peyret[1], Verena Kriechbaumer[3], Yohann Boutté[1], Jean-Jacques Bessoule[1,2] and Patrick Moreau[1,4,*]

[1] CNRS, University of Bordeaux, Laboratoire de Biogenèse Membranaire, UMR 5200, 33140 Villenave d'Ornon, France
[2] LEB Aquitaine Transfert-ADERA, INRA Bordeaux Aquitaine, 33140 Villenave d'Ornon, France
[3] Plant Cell Biology, Biological and Medical Sciences, Oxford Brookes University, Oxford OX3 0BP, UK
[4] Bordeaux Imaging Center, UMS 3420 CNRS, US004 INSERM, University of Bordeaux, 33000 Bordeaux, France

* Correspondence: patrick.moreau@u-bordeaux.fr

Received 8 June 2021; Editorial decision 9 November 2021; Accepted 16 November 2021

Editor: Angus Murphy, University of Maryland, USA

Abstract

Phosphatidic acid (PA) and lysophosphatidic acid acyltransferases (LPAATs) might be critical for the secretory pathway. Four extra-plastidial LPAATs (LPAAT2, 3, 4, and 5) were identified in *Arabidopsis thaliana.* These AtLPAATs display a specific enzymatic activity converting lysophosphatidic acid to PA and are located in the endomembrane system. We investigate a putative role for AtLPAATs 3, 4, and 5 in the secretory pathway of root cells through genetical (knockout mutants), biochemical (activity inhibitor, lipid analyses), and imaging (live and immuno-confocal microscopy) approaches. Treating a *lpaat4;lpaat5* double mutant with the LPAAT inhibitor CI976 produced a significant decrease in primary root growth. The trafficking of the auxin transporter PIN2 was disturbed in this *lpaat4;lpaat5* double mutant treated with CI976, whereas trafficking of H^+-ATPases was unaffected. The *lpaat4;lpaat5* double mutant is sensitive to salt stress, and the trafficking of the aquaporin PIP2;7 to the plasma membrane in the *lpaat4;lpaat5* double mutant treated with CI976 was reduced. We measured the amounts of neo-synthesized PA in roots, and found a decrease in PA only in the *lpaat4;lpaat5* double mutant treated with CI976, suggesting that the protein trafficking impairment was due to a critical PA concentration threshold.

Keywords: Arabidopsis, lysophosphatidic acid acyltransferase, lysophosphatidic acid, phosphatidic acid, PIN2; PIP2;7, roots, secretory pathway.

Introduction

Lipids are critical for organelle compartmentalization and membrane domain partition in all eukaryotic cells. In plant cells, the involvement of lipids and their metabolism in the regulation of the plant secretory pathway is evident (Melser *et al.*, 2011; Boutté and Moreau, 2014). It has been shown that all lipid families such as sterols (Laloi *et al.*, 2007; Men *et al.*, 2008; Boutté *et al.*, 2010), sphingolipids (Melser *et al.*, 2010; Markham *et al.*, 2011; Wattelet-Boyer *et al.*, 2016), and glycerolipids (Pleskot *et al.*, 2012; Boutté and Moreau, 2014) are involved in regulating the secretory pathway. *In vivo* and *in vitro* studies

in various eukaryotic models have shown that lipids play critical roles in regulation of endomembrane morphodynamics, organelle morphology, trafficking, as well as vesicle formation and fusion (Yang *et al.*, 2008, 2011; Ha *et al.*, 2012; Boutté and Moreau, 2014; Melero *et al.*, 2018).

A role for several enzymes in phospholipid metabolism such as phospholipases and lysophospholipid acyltransferases (LPATs) in the secretory/retrograde pathways has been particularly highlighted in animal and yeast cells (Yang *et al.*, 2008, 2011; Melero *et al.*, 2018). In plant cells, several phospholipases have been shown to be required for the functionality of the secretory pathway (Li and Xue, 2007; Lee *et al.*, 2010; Kim *et al.*, 2011; Li *et al.*, 2011). However, this is not the case for LPATs. Among LPATs, lysophosphatidic acid (LPA) acyltransferases (LPAATs) may be particularly crucial for the functionality of the secretory pathway as, in animal cells, phosphatidic acid (PA) and its precursor LPA have been shown to have an important impact on the functionality of the secretory pathway (Yang *et al.*, 2008, 2011). Therefore, PA and LPA, in addition to their role as precursors for *de novo* phospholipid biosynthesis and their known involvement in many signalling pathways (Pokotylo *et al.*, 2018; Yao and Xue, 2018), are of interest for the secretory pathway in plant cells.

The amount of cellular PA is dependent on the *de novo* synthesis via the Kennedy pathway but can be affected by the activity of multiple enzymes such as phospholipases D (PLDs), diacylglycerol kinases, or LPAATs. In addition, the sequential action of phospholipase C and a diacylglycerol kinase can increase the PA pool(s). In contrast, PA phosphatases or phospholipases A1/A2 cause a decrease in the amount of PA in the cells. A study carried out in *Nicotiana tabacum* indicated that pharmacological inhibition of most of these enzymes leads to very different effects on pollen tube growth (Pleskot *et al.*, 2012), indicating that there could be different PA pools related to different enzyme activities. At present, no studies have been conducted to specifically investigate the putative role of LPAATs in the secretory pathway of plant cells. We hypothesize that LPAATs could, as shown for phospholipases, participate in the regulation of membrane curvature by catalysing PA production from LPA (two molecules with different physicochemical properties) and therefore contribute to the regulation of membrane trafficking (Yang *et al.*, 2008, 2011; Boutté and Moreau, 2014).

In *Arabidopsis thaliana*, several membrane-bound LPAATs have been identified (Kim and Huang, 2004; Kim *et al.*, 2005; Wang *et al.*, 2013; Körbes *et al.*, 2016; Angkawijaya *et al.*, 2017, 2019). In higher eukaryotes, these enzymes are named LPAT or LPAAT, but here we propose to use the name LPAAT to precisely highlight their lysophosphatidic acid acyltransferase enzymatic activities. It is effectively inconsistent that the first identified isoform was named 'LPAAT1' whereas the subsequent isoforms were reported as 'LPAT2–LPAT5' (Kim *et al.*, 2005). AtLPAAT1 has been suggested to be involved in the *de novo* synthesis of PA in plastids (Kim and Huang, 2004; Yu *et al.*, 2004). The endoplasmic reticulum (ER)-located AtLPAAT2 (LPAT2; Kim *et al.*, 2005) has been shown to be critical for female gametophyte development in Arabidopsis (Kim *et al.*, 2005). In addition, the overexpression of AtLPAAT2, which stimulates the *de novo* production of phospholipids, resulted in enhanced primary root growth in phosphate-starved Arabidopsis seedlings (Angkawijaya *et al.*, 2017). This suggests AtLPAAT2 to be a primordial enzyme for the *de novo* synthesis of PA in the ER. Three other potential LPAAT genes, *AtLPAAT3*, *AtLPAAT4*, and *AtLPAAT5*, have been identified. Recently, Angkawijaya *et al.* (2019) have shown that AtLPAAT4 and AtLPAAT5 can be involved in the neo-synthesis of phospholipids and triglycerides in response to nitrogen starvation. Since AtLPAAT2 is probably the main source of PA for the *de novo* synthesis of phospholipids (Kim *et al.*, 2005; Angkawijaya *et al.*, 2017), we have investigated whether other AtLPAATs can be associated with a further role in membrane dynamics linked to the functionality of the secretory pathway.

We first showed that these AtLPAATs have an enzymatic activity specific for producing PA from LPA and that they are located in the endomembrane system (mainly the ER). Through genetic, biochemical, and imaging approaches, we show that a *lpaat4;lpaat5* double mutant is sensitive to salt stress and is defective in primary root growth when treated with the LPAT inhibitor CI976 (Brown *et al.*, 2008; Schmidt and Brown, 2009; Yang *et al.*, 2011). In addition, the trafficking of the aquaporin PIP2;7 and the auxin carrier PIN2 is affected in these mutants. By measuring the amounts of PA in the roots, we were able to link the disturbance of protein trafficking to a critical PA concentration threshold.

Materials and methods

Arabidopsis material and growth conditions

The *A. thaliana* ecotype Colombia-0 (Col-0) and the following mutants were used: *lpaat3-1* (SALK_046680), *lpaat4-2* (GK_899A04), and *lpaat5-2* (SALK_020291). Double mutants *lpaat3-1;lpaat4-2*, *lpaat3-1;lpaat5-2*, and *lpaat4-2;lpaat5-2* were obtained crossing the previously listed lines. The triple mutant *lpaat3-1;lpaat4-2;lpaat5-2* was obtained crossing the double mutant *lpaat4-2;lpaat5-2* and SALK_046680. The transgenic green fluorescent protein (GFP) marker line pPIN2::PIN2–GFP (in Col-0; Xu and Scheres, 2005) was crossed with the double mutant *lpaat4-2;lpaat5-2*.

Seeds were sterilized by treatment with 95% (v/v) ethanol for 10 s, followed by a bleach solution for 20 min, then repeatedly washed with sterile water. Seeds were then sown on 1/2 Murashige and Skoog (MS) agar medium plates [0.8% plant agar (Meridis #P1001,1000), 1% sucrose (Merck # 84100), and 2.5 mM MES (Euromedex # EU0033) pH 5.8 with KOH], left at 4 °C for 2 d, and then grown vertically in 16 h light/8 h darkness for 5 d.

Inhibitor treatment

CI976 was used as a LPAT inhibitor (Merck # C3743). A 10 mM CI976 stock solution was prepared in DMSO, and stored at –20 °C. Seedlings were grown on 1/2 MS plates containing 10 μM of the inhibitor for all experiments, except to determine the sensitivity of the wild-type (WT), double mutant *lpaat4-2;lpaat5-2*, and triple mutant

lpaat3-1;lpaat4-2;lpaat5-2 lines to the treatment, where 5 μM of inhibitor was also tested. In all experimental conditions, the final DMSO concentration was the same for the controls without CI976 and at the different concentrations of CI976 used.

Phenotypical characterization

Seedlings were grown on 1/2 MS agar medium plates containing varying CI976 concentrations (0, 5, or 10 μM). Root length was measured 5 d after germination using the ImageJ software. To compare experiments, all the measured values were standardized to the WT median value in untreated condition for each experiment.

To assess the sensitivity of the different lines to salt stress, 50 mM NaCl (Euromedex # 1112) was added to the 1/2 MS agar medium.

Plasmid preparation and transgenic plants

Sequence data of AtLPAATs can be found in the Arabidopsis Genome Initiative or GenBank/EMBL databases under the following accession numbers: *AtLPAAT2*, At3g57650; *AtLPAAT3*, At1g51260; *AtLPAAT4*, At1g75020; and *AtLPAAT5*, At3g18850. The coding sequences of *AtLPAAT2* and *AtLPAAT4* were amplified on leaf cDNA, while those of *AtLPAAT3* and *AtLPAAT5* were amplified on flower cDNA. We used the primer pairs P1531/P1533, P1539/P1541, P1535/P1537, and P1543/P1545, respectively. To generate the following di=lysine (diK) mutants: *AtLPAAT2 K387A/K389A*, *AtLPAAT4 K374A/K376A*, and *AtLPAAT5 K371A/K375A*, the following primer pairs containing the mutation were used: P5294/P5431, P2051/P2052, and P5292/P5432. *LPAAT3* diacidic mutant 1 (D74G/A75/E76G) and 2 (D293G/L294A/E295G) were obtained by overlapping PCR using primers P2578/P2580/P2581/P2582/P66/P67 and P2578/P2580/P2585/P2586/P66/P67, respectively. Amplified sequences were cloned by BR reactions in entry vectors pDONR™221 or pENTR-d-TOPO™ (Thermofisher Scientific) using Gateway® recombinational cloning technology (Thermofisher Scientific). For expression in *Escherichia coli*, entry vectors were cut by *Nco*I (Biolabs #R0193) and *Xho*I (Biolabs #R0146) restriction endonucleases. The product was cloned into the pET-15b vector (Novagen). For expression in plant, AtLPAAT entry vectors and pK7WGF2 destination vectors were combined by LR recombination using Gateway® recombinational cloning technology (Thermofisher Scientific).

To complement the double mutant *lpaat4-2;lpaat5-2*, we generated the construct p*AtLPAAT4*:tagRFP-*AtLPAAT4g*. For that, we amplified the *AtLPAAT4* promoter sequence and the *AtLPAAT4* full-length DNA genomic sequence using the primer pairs P5730/P5731 and P5736/5737. Each PCR product was purified and cloned in pDONR™ P4-P1r vector and pDONR™ P2r-P3 vector (Thermofisher Scientific), respectively. We used a third vector containing tagRFP (red fluorescent protein) in the pDONR™221 backbone (Thermofisher Scientific) and generated the final construct in the pH7m34GW destination vector using the Multisite Gateway® cloning system (Thermofisher Scientific).

All PCR amplifications were performed using Q5™ High-Fidelity DNA polymerase at the annealing temperature and extension times recommended by the manufacturer (Biolabs #M04915). PCR fragments and plasmids were respectively purified with NucleoSpin® Gel and PCR cleanup (Macherey-nagel # 740609) and NucleoSpin® Plasmid (Macherey-Nagel #740499). All the entry vectors were sequenced, and sequences were analysed with CLC Mainwork Bench 6. Primers used in this study are listed in Supplementary Table S1.

For transient expression in Arabidopsis cotyledons, seeds were sterilized as described above and sown in 6-well culture plates containing 4 ml of 1/2 MS agar medium. Plates were left at 4 °C for 2 d and then grown in 16 h light/8 h darkness for 7 d.

Constructs were transferred into the *Agrobacterium tumefaciens* C58C1Rif^{R} strain harbouring the plasmid pMP90. At 4 d after germination, *A. tumefaciens* suspension in MS-Glu liquid medium [0.21% MS (w/v), 2% glucose (w/v), 0.39% MES (w/v), 0.05% Tween, 200 mM acetosyringone, pH 5.7] was used to transiently transform the cotyledons. For that, seedlings were incubated for 40 min at room temperature with a suspension of *A. tumefaciens* expressing native or mutant LPAATs and the HDEL marker at 1 $OD_{600\ nm}$ and 0.2 $OD_{600\ nm}$, respectively. The suspension was then removed and the plate were left in 16 h light/8 h darkness until the seventh day after germination.

To study the effect of the double mutation *lpaat4-2;lpaat5-2* on PIN2–GFP subcellular localization at the plasma membrane, the double mutant *lpaat4-2;lpaat5-2* and the pPIN2::PIN2–GFP transgenic line (Xu and Scheres, 2005) were crossed. Primer pairs 1905/1906 (LP/RP SALK-020291), 5744/5745 (LP/RP GABI_899A04), and LBa1 were used for genotyping on ammonium glufosinate- (10 μg ml^{-1}) resistant seedlings.

RNA extraction, RT–PCR, and qPCR

Tissues were disrupted using 5 mm stainless steel beads (Qiagen#69989) and Tissuelyser II (Qiagen). Total RNA was extracted from roots 5 d after germination using the RNeasy® Plant Mini kit (Qiagen #74904) according to the manufacturer's instructions. First-strand cDNA was synthesized using SuperScript® II Reverse Transcriptase (ThermoFisher # 18064014) and oligo(dT). Then, mRNAs were treated with DNase I using the DNa-*free*™ Kit (ThermoFisher # AM1906). Analyses of expression of *AtLPAAT2*, *AtLPAAT3*, *AtLPAAT4*, and *AtLPAAT5* by quantitative reverse transcription–PCR (RT–qPCR) was performed with the Bio-Rad CFX96 real-time system using GoTaq® qPCR Master mix (Promega # A6002). The specific primer pairs used for *AtLPAAT2*, *AtLPAAT3*, *AtLPAAT4*, *AtLPAAT5*, *EF-1α*, and *At4g33380* were P5412/P5413, P5414/P5415, P5783/P5784, P5418/P5419, P4833/P4834, and P4847/P4848, respectively.

The transcript abundance in samples was determined using a comparative cycle threshold (C_t) method. The relative abundance of *EF-1α* and *At4g33380* mRNAs (Czechowski *et al.*, 2005) in each sample was determined and used to normalize for differences of total RNA level as described in Pascal *et al.* (2013). Semi-quantitative RT–PCR analysis of steady-state At*LPAAT* gene transcripts in roots from 5 day-old-plants was performed to compare all the mutant lines with WT plants. The *EF-1α* gene was used as a constitutively expressed control. We used GoTaq® G2 DNA Polymerase (Promega). All primers are listed in Supplementary Table S1, the characterization of *lpaat* insertion mutant lines and T-DNA positions is shown in Supplementary Fig. S1, and controls for all the mutant lines are shown in Supplementary Fig. S2.

Immunocytochemistry, FM4-64 uptake, BFA treatment, and confocal laser scanning microscopy

Whole-mount immunolabelling of Arabidopsis roots was performed as described in Boutté and Grebe (2014). In brief, 5-day-old seedlings were fixed in 4% paraformaldehyde dissolved in MTSB (50 mM PIPES, 5 mM EGTA, 5 mM $MgSO_4$ pH 7 with KOH) for 1 h at room temperature and washed three times with MTSB. Roots were cut on superfrost slides (Menzel Gläser, Germany) and dried at room temperature. Roots were then permeabilized with 2% Driselase (Merck #D9515), dissolved in MTSB for 30 min at room temperature, rinsed four times with MTSB, and treated for 1 h at room temperature with 10% DMSO+3% Igepal CA-630 (Merck # I3021) dissolved in MTSB. Unspecific sites were blocked with 5% normal donkey serum (NDS; Merck # D9663) in MTSB for 1 h at room temperature. Primary antibodies, in 5% NDS/MTSB, were incubated overnight at 4 °C and then washed four times with MTSB. Secondary antibodies, in 5% NDS/MTSB, were incubated for 1 h at room temperature and then washed four times with MTSB.

Primary antibodies were diluted as follows: rabbit anti-PIP2;7 1:400 (Agrisera, AS09469), rabbit anti-H^+-ATPase 1:1000 (Agrisera AS07260),

rabbit anti-echidna 1:600 (Gendre *et al.*, 2011; Boutté *et al.*, 2013), rabbit anti-Membrine11 1:300 (Marais *et al.*, 2015), and rabbit anti-SAR1 1:250 (Agrisera AS08326). Dilution of secondary antibody AlexaFluor 488-coupled donkey anti-rabbit IgG (Jackson Immunoresearch, 711-605-152) was 1:300.

FM4-64 uptake was performed on 5-day-old seedling that had grown on 1/2 MS agar medium containing 10 μM CI976. Seedlings were dark incubated in 5 μM FM4-64 solution for 5 min. A rapid wash in 1/2 MS solution containing 10 μM CI976 followed, and FM4-64 uptake was determined each minute on root epidermal cells by confocal microscopy from 3 min to 15 min after seedlings wash. For brefeldin A (BFA) treatment, 5-day-old seedlings grown on 1/2 MS agar medium supplemented with 10 μM CI976 were incubated in liquid 1/2 MS medium with 10 μM CI976 and 50 μM BFA (Merck B7651). After 90 min of incubation, PIN2 accumulation in BFA bodies was determined in roots by confocal microscopy.

Confocal laser scanning microscopy was performed using a Zeiss LSM880 microscope. For live-cell imaging, seedlings were mounted with MS liquid medium. Laser excitation lines for the different fluorophores were 488 nm for GFP, AlexaFluor 488, and FM4-64, and 561 nm for mCherry. Fluorescence emissions were detected at 490–570 nm for GFP and AlexaFluor 488, 620–695 nm for FM4-64, and 580–660 nm for mCherry. Scanning was performed with a pixel dwell of 3 μs. In multilabelling acquisitions, detection was in sequential line-scanning mode. An oil-corrected ×63 objective, numerical aperture=1.4 (C Plan Apochromat ×63.0, 1.40 OIL DIC UV VIS IR-M27) was used in immunolabelling and live-cell imaging experiments, except for FM4-64 uptake where an oil-corrected ×40 objective, numerical aperture=1.3 (Plan Apochromat ×40.0, 1.3 OIL DIC UV IR-M27) was used. Image analysis was performed using ZEN lite 2.6 2018 (Zeiss) and ImageJ software.

Tobacco leaf infiltration and confocal microscopy

Nicotiana tabacum (SR1 cv Petit Havana) plants were grown in a greenhouse for transient expression of fluorescent constructs according to Sparkes *et al.* (2006). In brief, each expression vector was introduced into *A. tumefaciens* strain GV3101 by heat shock transformation. Transformed colonies were inoculated into 5 ml of YEB medium (5 g l^{-1} beef extract, 1 g l^{-1} yeast extract, 5 g l^{-1} sucrose, and 0.5 g l^{-1} $MgSO_4 \cdot 7H_2O$) with 50 μg ml^{-1} spectinomycin and rifampicin. The bacterial culture was incubated overnight in a shaker at 180 rpm at 25 °C. A 1 ml aliquot of the bacterial cultures was pelleted by centrifugation at 1800 *g* at room temperature for 5 min. Pellets were washed with infiltration buffer (5 mg ml^{-1} glucose, 50 mM MES, 2 mM $Na_3PO_4 \cdot 12H_2O$, and 0.1 mM acetosyringone) and then resuspended in infiltration buffer. The bacterial suspension was diluted in infiltration buffer to a final OD_{600} of 0.1 for each construct. The bacterial solution was injected into the underside of the tobacco leaf using a 1 ml syringe. Infiltrated plants were incubated at 22 °C for 3 d prior to imaging. Leaf epidermal samples were imaged using a Zeiss PlanApo ×100/1.46 NA oil immersion objective on a Zeiss LSM880 confocal microscope equipped with an Airyscan detector. Images of 512×512 pixels were collected in 8-bit with four-line averaging. For GFP, excitation was set at 488 nm and emission at 495–550 nm; and for RFP at 561 nm and 570–615 nm, respectively.

AtLPAAT enzymatic activity

The ORFs for *AtLPAAT2–AtLPAAT5* were amplified by PCR with the sense/antisense primers P1539/1541 and P1543/1545 containing, respectively, the *Xho*I and *Nco*I restriction sites. The PCR products were first subcloned in pGEM®-T Easy vector (Promega, Charbonnieres les Bains, France) before being cloned into the *Xho*I/*Nco*I sites of the pET-15 vector (Novagen, Merck Biosciences, Badsoden, Germany). C41 (DE3) *E. coli* bacteria (Avidis, Saint-Beauzire, France) were then transformed with the obtained plasmids. Ectopic expression of the ORFs of *AtLPAAT2–5* and *E. coli* membrane isolation were performed as described by Testet *et al.* (2005). *AtLPAAT2–AtLPAAT5* were produced in membranes of the *E. coli* C41 cell line that was specifically designed for the production of membrane proteins (Miroux and Walker, 1996). Lysophospholipid acyltransferase reactions were carried out in 100 μl of assay mixtures (50 mM Tris–HCl, pH 8) containing 1 nmol of LPA or the other lysophospholipids (either lysolysophosphatidylcholine, lysophosphatidylethanolamine, lysophosphatidylglycerol, lysophosphatidylinositol, or lysophosphatidylserine), 1 nmol of [^{14}C] oleoyl-CoA, and 50 μg of membrane proteins. Reactions were incubated at 30 °C and stopped at 30 min by adding 2 ml of chloroform/methanol (2:1, v/v) and 500 μl of water. After the isolation of the organic phase, the aqueous phase was re-extracted with 2 ml of chloroform. The lipids were then purified by high-performance TLC (HPTLC) according to Testet *et al.* (2005) and Ayciriex *et al.* (2012). The radioactivity incorporated into phospholipids was revealed using a STORM 860 PhosphorImager (GE Healthcare, Waukesha, WI, USA) and quantified with ImageQuant TL software.

LPAAT activities were measured as nmol phospholipids formed mg $proteins^{-1}$ 30 min^{-1}, the values of the controls (corresponding to purified membranes from *E. coli* transformed with pET-15B empty vector) were normalized to 100 for each lysophospholipid and the corresponding activities for LPAAT2–LPAAT5 were calculated accordingly for all the phospholipids. Values of the controls were normalized to 100 to take into account the variations observed in the activity levels between experiments; this allowed the best conditions to compare data and to perform the statistical analysis.

[^{14}C]Acetate labelling and lipid analysis

For radiolabel feeding experiments, 20 roots of 5-day-old seedlings were cut with a razor blade and placed in vials containing 2 ml of MS. To start the reaction, 200 nmol (10 μCi) of [1-^{14}C]acetate (Perkin Elmer Life Sciences) were added to each vial and the reaction was stopped after 4 h with 2 ml of pre-heated isopropanol followed by 20 min incubation at 70 °C. After transfer into 6 ml glass tubes, 2 ml of chloroform/methanol/hydrochloric acid (100:50:1; v/v/v) were added and the mixture was incubated overnight on an orbital rotator (40 rpm) at room temperature. Subsequently, each tube was centrifuged at 1000 *g* for 10 min. The organic phase was collected in new tubes and the roots were re-extracted with 2 ml of chloroform/methanol (2:1, v/v) for 2 h. After re-centrifugation, the organic phases of each sample were combined, mixed with 1.5 ml of 0.9% NaCl, and centrifuged at 1000 *g* for 10 min. The organic phases were evaporated to dryness, re-suspended in 40 μl of chloroform/methanol (2:1, v/v), and stored at −20 °C. Radiolabelled products were analysed by TLC using HPTLC Silica Gel 60 plates (Merck) and chloroform/methanol/water/acetic acid (30:17:2:1, v/v/v/v) as solvent to separate phospholipids. They were identified by co-migration with unlabelled standards, and quantification was done by autoradiography using a Storm 860 molecular imager (GE Healthcare).

Statistical analysis

All data analysed were unpaired (samples independent from each other). Normal distribution (Gaussian distribution) of the dataset was tested using Shapiro–Wilk normality test. On data normally distributed, sample homoscedasticity was assessed using a Bartlett test before performing parametric tests. On data that were not normally distributed (or on datasets for which n <10), non-parametric tests were performed. To compare two datasets, Welch two-sample t-tests were performed on normally distributed datasets, whereas Mann–Whitney test was used as the non-parametric test. To compare multiple datasets, Kruskal–Wallis tests

were used as the non-parametric test. Tukey's test was used as a single-step multiple comparison procedure to find means significantly different from each other. All statistical tests were two-tailed (two-sided test). All statistical analyses were performed with the R i386 3.1.0 software. *P*-values were as follows: ^{NS}P-value >0.01 (not significant), $*P<0.05$, $**P<0.01$, and $***P<0.001$.

Results

In vitro *AtLPAAT activities in* E. coli *C41 membranes*

Supplementary Fig. S3 shows the alignment of the amino acid sequences of AtLPAAT2–AtLPAAT5 from Arabidopsis with the sequence of the human LPAAT3 (Schmidt and Brown, 2009). The boxes indicate conserved sequences which correspond to classical motifs of the LPAAT, DHAPAT, and LPEAT acyltransferase families (Lewin *et al.*, 1999), indicating that AtLPAAT2–AtLPAAT5 are clearly acyltransferases. In *E. coli* and yeast expression systems, AtLPAAT2 and AtLPAAT3 showed lysophosphatidic acid acyltransferase activity but AtLPAAT4 and AtLPAAT5 did not (Kim *et al.*, 2005). Recently, Angkawijaya *et al.* (2019) showed lysophosphatidic acid acyltransferase activity for AtLPAAT5 expressed in *E. coli* C41 cells but not for AtLPAAT4 using this expression system. They identified AtLPAAT4 activity upon overexpression in *A. thaliana* plants. However, it is still unknown whether these enzymes only utilize LPA or whether they can also handle other lysophospholipids as substrates. To investigate this, AtLPAAT2–AtLPAAT5 were expressed in membranes of an *E. coli* C41 cell line specifically designed for the production of membrane proteins (Miroux and Walker, 1996), and activities were measured *in vitro* as described in the Materials and methods and according to Testet *et al.* (2005). Purified membranes of *E. coli* C41 cells were incubated with LPA or the other lysophospholipids (lysophosphatidylcholine, lysophosphatidylethanolamine, lysophosphatidylglycerol, lysophosphatidylinositol, or lysophosphatidylserine) and [^{14}C] oleoyl-CoA to measure the formation of either [^{14}C]PA or the other potentially labelled phospholipids [phosphatidylcholine (PC), phosphatidylethanolamine (PE), phosphatidylglycerol, phosphatidylinositol, or phosphatidylserine]. Purified membranes from *E. coli* transformed with a pET-15B empty vector were used as controls to measure *E. coli* endogenous activities. Lysophospholipid acyltransferase activities were measured as nmol phospholipids formed mg proteins^{-1} 30 min^{-1}, the values of the controls were normalized to 100 for each lysophospholipid, and the corresponding activities for AtLPAAT2–AtLPAAT5 were calculated accordingly for all the phospholipids.

Figure 1 shows the mean enzymatic activities of AtLPAAT2–AtLPAAT5 from three independent experiments. Only LPA acyltransferase activities were detected for AtLPAAT2–AtLPAAT5 and no other lysophospholipid acyltransferase activity was observed, demonstrating that the four AtLPAATs are clearly strict lysophosphatidic acid acyltransferases. It was a

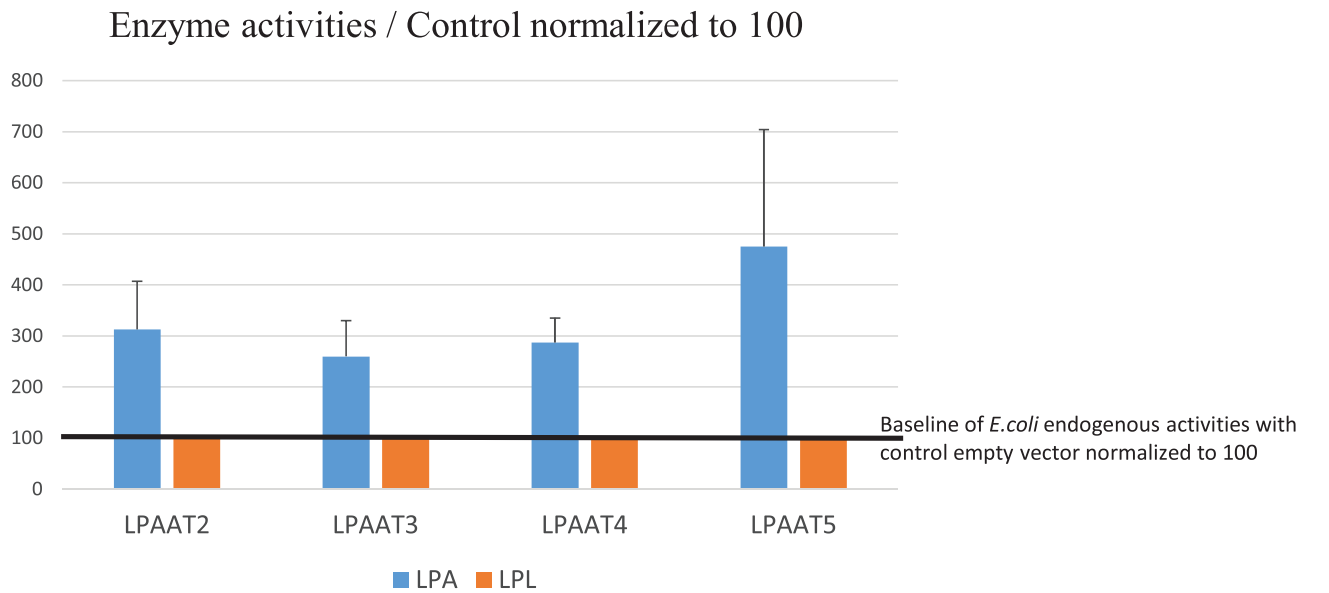

Fig. 1. *In vitro* AtLPAAT2–AtLPAAT5 lysophosphatidic acid (LPA) acyltransferase activities in *E. coli* C41 membranes. *AtLPAAT2–AtLPAAT5* were produced in membranes of an *E. coli* C41 cell line that was specifically designed for the production of membrane proteins (Miroux and Walker, 1996), and activities were measured *in vitro* as described in the Materials and methods and according to Testet *et al.* (2005). Activities were tested with LPA and the other lysophospholipids (LPL: either lysophosphatidylcholine, lysophosphatidylethanolamine, lysophosphatidylglycerol, lysophosphatidylinositol, or lysophosphatidylserine). Lysophospholipid acyltransferase activities were measured as nmol phospholipids formed mg proteins^{-1} 30 min^{-1}, the values of the controls (corresponding to purified membranes from *E. coli* transformed with pET-15B empty vector) were normalized to 100 for each lysophospholipid, and the corresponding activities for AtLPAAT2–AtLPAAT5 were calculated accordingly for all the phospholipids. Only LPA acyltransferase activities were detected for AtLPAAT2–AtLPAAT5, and no other lysophospholipid acyltransferase activity was detected, determining that AtLPAAT2–AtLPAAT5 are strict LPA acyltransferases.

very important point to determine in order to investigate the potential role of PA synthesized by these enzymes in the functionality of the secretory pathway.

The activities of PA synthesis were calculated as 1.25 nmol PA mg proteins^{-1} 30 min^{-1} for AtLPAAT2, 1.08 nmol PA mg proteins^{-1} 30 min^{-1} for AtLPAAT3, 1.72 nmol PA mg proteins^{-1} 30 min^{-1} for AtLPAAT4, and 1.75 nmol PA mg proteins^{-1} 30 min^{-1} for AtLPAAT5. This indicated similar levels of activities in *E. coli* C41 cell membranes, which does not necessarily reflect their level of activities *in planta*.

Subcellular localization of AtLPAATs in Arabidopsis

AtLPAAT2, 4, and 5 have previously been shown to be located in the ER (Kim *et al.*, 2005; Angkawijaya *et al.*, 2019). However, the subcellular localization of AtLPAAT3 has not been determined. To investigate its membrane localization, roots of an Arabidopsis stable line (5 d after germination) expressing both GFP–LPAAT3 and the ER marker mCherry–HDEL were analysed using high-resolution confocal microscopy (Fig. 2). In contrast to AtLPAAT2, 4, and 5, GFP–AtLPAAT3 was not localized to the ER network but labelled round structures in close proximity to the ER (Fig. 2A–F). We further investigated the localization of AtLPAAT3 using a heterologous expression system in tobacco leaf epidermal cells in which the ER is more dynamic and accessible than in root cells. Interestingly, here tagRFP–AtLPAAT3 and the ER export sites (ERES) marker SAR1a–GFP co-localized (Fig. 2G–I). This indicates that AtLPAAT3 may localize to ERES also in Arabidopsis roots. The AtLPAAT3 amino acid sequence indeed features

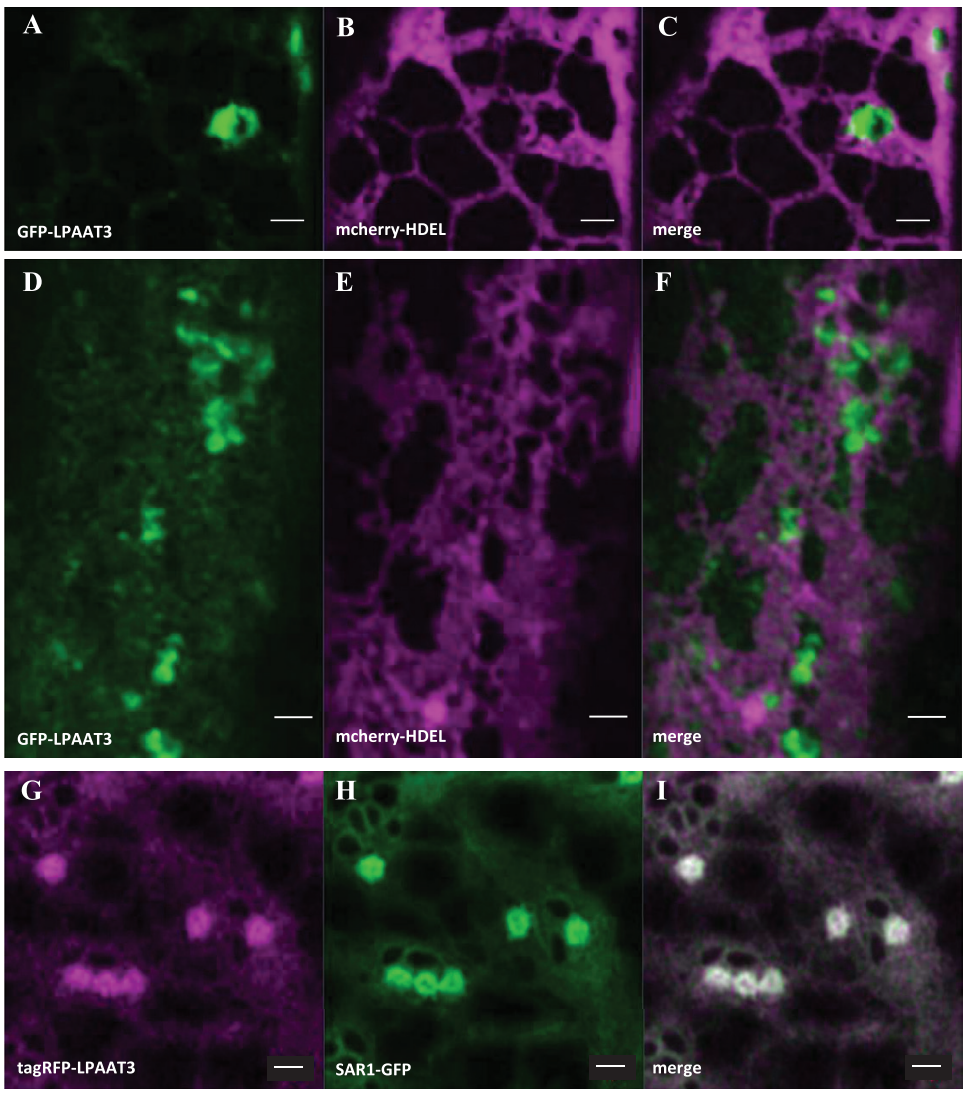

Fig. 2. Subcellular localization of AtLPAAT3 in various plant models. Roots, 5 d after germination, of an Arabidopsis stable line expressing both GFP–LPAAT3 (A, D) and the ER marker mCherry–HDEL (B, E). AtLPAAT3 was found in punctate structures in close proximity to the ER (C, F). A transient expression of tagRFP–LPAAT3 (G) and the ERES marker SAR1a–GFP (H) in *Nicotiana tabacum* leaf epidermis cells suggested that the punctate structures observed for AtLPAAT3 in roots could potentially correspond to ERES (I). Scale bars=1 μm.

di-acidic motifs (D74-X-E76 and D293-X-E295) which could serve as ER export signals and may explain the different localization compared with the other LPAATs. Transient expressionof GFP–LPAAT3 di-acidic mutants 1 (D74G/A75/E76G) and 2 (D293G/L294A/E295G) in Arabidopsis cotyledons together with the ER marker mCherry–HDEL showed significant redistribution of both mutant AtLPAAT3s from to the ER network (Fig. 3), indicating that these motifs may be functional.

AtLPAAT2, AtLPAAT4, and AtLPAAT5 do not cycle between the ER and the Golgi

As shown in Supplementary Fig. S3, AtLPAAT2, AtLPAAT4, and AtLPAAT5, but not AtLPAAT3, feature potential di-lysine motifs at their C-termini (KXK, KXKXX, and KXXXK motifs, respectively). Although these motifs are not very typical di-lysine motifs, they may indicate that the enzymes could potentially cycle between the ER and Golgi/post-ER compartments. To investigate this possibility, we mutated the potential cycling motifs (GFP–LPAAT2 *K387A/K389A*, GFP–LPAAT4 *K374A/K376A*, and GFP–LPAAT5 *K371A/K375A*) and expressed these mutant fluorescent constructs in Arabidopsis cotyledons together with the ER marker mCherry–HDEL. As shown in Fig. 4, all the mutated versions of AtLPAAT2, AtLPAAT4, and AtLPAAT5 were still located in the ER and did not label any round structures which could correspond to Golgi/post-ER compartments. Therefore, removing the C-terminal di-lysine motifs did not affect protein localization, indicating that these enzymes do not cycle between the ER and the Golgi or post-ER compartments, excluding any role for these proteins at the level of the Golgi membranes.

Since AtLPAAT2 is most probably the main enzyme responsible for *de novo* synthesis of phospholipids in the ER (Kim *et al.*, 2005; Angkawijaya *et al.*, 2017), AtLPAAT3, 4, and 5 were investigated for involvement in the ER trafficking machinery and their importance for the secretory pathway. Since AtLPAAT3–AtLPAAT5 are expressed at similar levels in roots (Supplementary Fig. S4), we chose primary root growth as a phenotypic readout for the functionality of the secretory pathway.

Primary root growth phenotype and sensitivity to Cl976 of lpaat *mutants*

Since an *AtLPAAT2* knockout (KO) mutant is lethal (Kim *et al.*, 2005), we first looked at the primary root growth of the

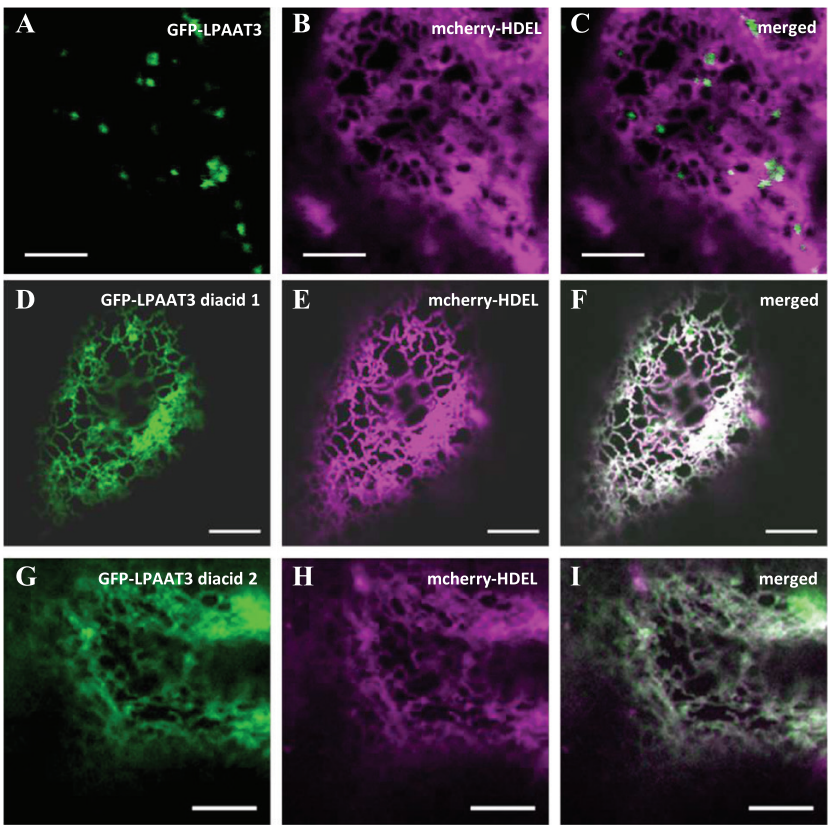

Fig. 3. Subcellular localization of AtLPAAT3 depends on active ER export motifs. Transient expression of LPAAT3 GFP-fused native forms (A), GFP–LPAAT3 di-acidic mutant 1 (D), GFP–LPAAT3 di-acidic mutant 2 (G), and the ER marker mCherry–HDEL (B, E, H) in Arabidopsis cotyledons. The mutation of each diacidic motif induces redistribution of LPAAT3 into the ER network (F, I) compared with the control (C). Scale bars=5 μm.

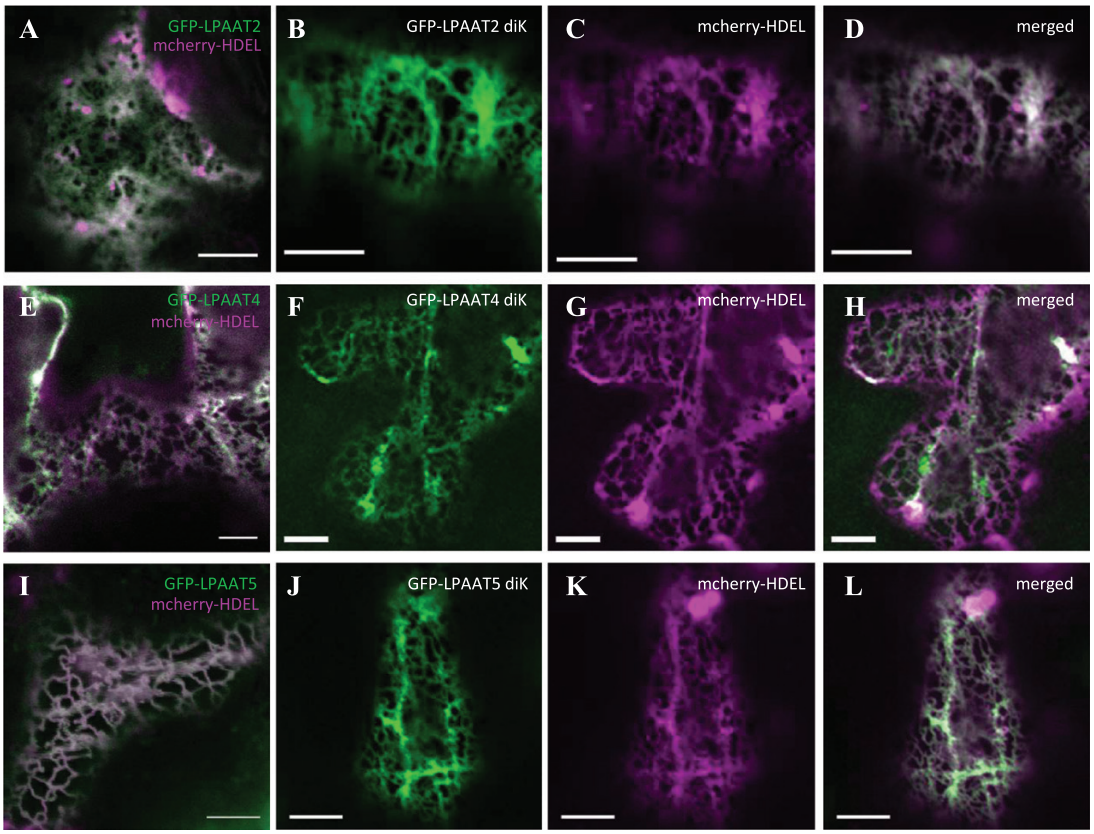

Fig. 4. AtLPAAT2, AtLPAAT4, and AtLPAAT5 do not cycle between the ER and the Golgi. Transient expression of the GFP–LPAAT2 diK mutant (B), GFP–LPAAT4 diK mutant (F), GFP–LPAAT5 diK mutant (J), and the ER marker mCherry–HDEL (C, G, K) in Arabidopsis cotyledons. Results are compared with transient co-expression of GFP-fused native forms of AtLPAAT2 (A), AtLPAAT4 (E), and AtLPAAT5 (I) with the ER marker mCherry–HDEL. Mutations of AtLPAAT2, AtLPAAT4, and AtLPAAT5 diK motifs do not impact their location to the ER network (D, H, L). Scale bars 5μm.

single KO mutants *lpaat3-1* (Angkawijaya *et al.*, 2017), *lpaat4-2*, and *lpaat5-2* (different alleles from those used by Angkawijaya *et al.*, 2019) 5 d after germination. The characterization of *lpaat* insertion mutant lines and T-DNA positions is shown in Supplementary Fig. S1. As shown in Fig. 5A, none of these mutants had a decrease in their primary root growth which could be due to complementation by other AtLPAAT proteins (representative images of seedlings are shown in Supplementary Fig. S5). Therefore, we produced the three double mutants *lpaat3-1;lpaat4-2*, *lpaat3-1;lpaat5-2*, and *lpaat4-2;lpaat5-2*, and analysed the primary root length 5 d after germination (Fig. 5B). A significant but weak root length phenotype was observed for all the double mutants (see also Supplementary Fig. S5 for representative images). As a consequence, we decided to produce the triple mutant *lpaat3-1;lpaat4-2;lpaat5-2* and analysed the primary root length again in these mutant plants. Surprisingly, primary growth was not inhibited but stimulated in the triple mutant (Supplementary Fig. S6). Since the overexpression of *AtLPAAT2* stimulates the *de novo* synthesis of phospholipids, resulting in an enhanced primary root growth in phosphate-starved Arabidopsis seedlings (Angkawijaya *et al.*, 2017), we wondered whether the expression of *AtLPAAT2* was increased in the triple mutant *lpaat3-1;lpaat4-2;lpaat5-2*. To check this hypothesis, semi-quantitative RT–PCR and real-time RT–PCR analyses of *AtLPAAT2* transcripts were performed in roots 5 d after germination (Supplementary Fig. S7). In comparison with WT plants, the transcription of *AtLPAAT2* was indeed increased in the triple mutant *lpaat3-1;lpaat4-2;lpaat5-2* but not in the double mutant *lpaat4-2;lpaat5-2*. This indicates that *AtLPAAT2* is overexpressed in the triple mutant *lpaat3-1;lpaat4-2;lpaat5-2*, and could compensate for the absence of the three other AtLPAATs, resulting in an increase in primary root growth. The triple mutant also contained the same level of PA as WT plants Fig. 7A). We attempted an inducible RNAi approach to knock down the expression of LPAAT2 in the triple mutant background to check whether this could restore the phenotype to the *lpaat4-2;lpaat5-2* double mutant. Unfortunately, either the drop in the expression was too low to observe a phenotype, or a lethal phenotype was observed, and no lines were obtained with intermediary conditions for such an approach to be possible.

This raises the question of how to investigate a putative role for AtLPAATs in the secretory pathway with double mutants showing only a weak growth inhibition phenotype and a triple mutant showing even an increase in primary root growth. To address this, we took advantage of our experience

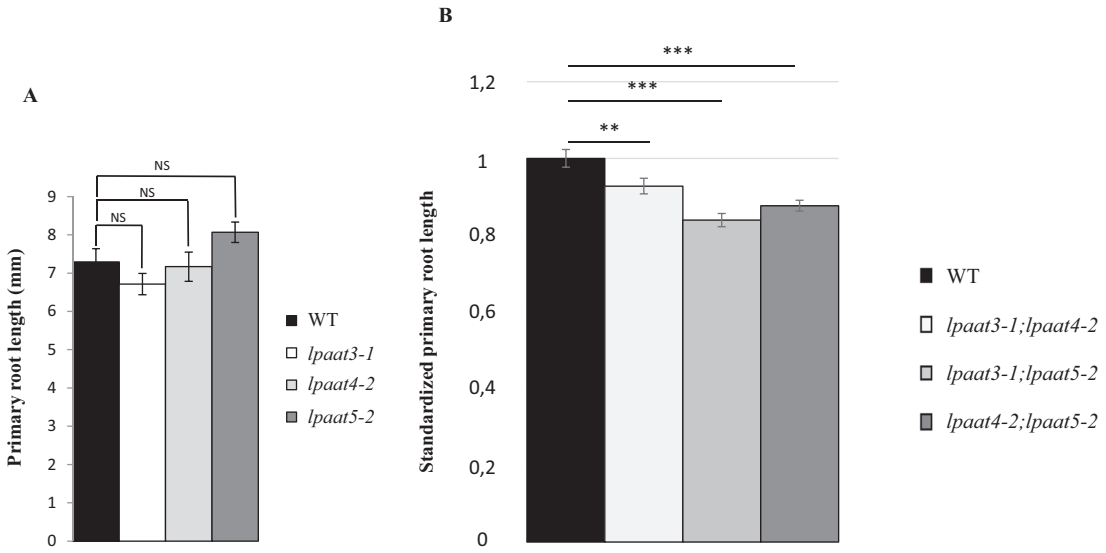

Fig. 5. Primary root growth of *lpaat* KO mutants (A) is not impaired and that of *lpaat* KO double mutants (B) is significantly but only slightly impaired. Primary root length was measured 5 d after germination. Data are mean values ±SE, *n*=40 (*lpaat* KO mutants), *n*=80 (*lpaat* KO double mutants). Statistics were done by Kruskal–Wallis rank sum test, NS=not significant, ***P*<0.01, ****P*<0.001.

in combining genetic and biochemical approaches used in investigating the role of sphingolipids in protein trafficking at the Golgi body (Melser *et al.*, 2010; Wattelet-Boyer *et al.*, 2016). CI976 is an inhibitor of LPAT enzyme activities that interferes with both COPII- and COPI-dependent membrane traffic processes (Brown *et al.*, 2008; Schmidt and Brown, 2009; Yang *et al.*, 2011). The effects of this inhibitor on primary root growth were analysed in the double mutant *lpaat4-2;lpaat5-2* (with no increase in the transcription of AtLPAAT2) and the triple mutant *lpaat3-1;lpaat4-2;lpaat5-2*. The double mutant *lpaat4-2;lpaat5-2* was chosen for this study as both AtLPAAT4 and AtLPAAT5 localize to the ER and therefore the inhibitor would affect the ER.ES-localized AtLPAAT3. A small but statistically not significant decrease in primary root growth was observed in WT plants. The triple mutant *lpaat3-1;lpaat4-2;lpaat5-2-* was not affected by the inhibitor, which was expected due to overexpression of *AtLPAAT2*. A significant decrease in primary root growth was observed in the double mutant *lpaat4-2;lpaat5-2* treated with 10 µM CI976 (Fig. 6; representative images of seedlings shown in Supplementary Fig. S5). Higher concentrations of CI976 induced a decrease in primary root growth in WT and mutant lines, justifying 10 µM as the functional concentration of the inhibitor CI976 for these assays. We also checked whether the inhibitor could enhance the transcription of *AtLPAAT2*. Here transcription was similarly increased in the WT and in the double mutant *lpaat4-2;lpaat5-2* but to a much lesser extent than in the triple mutant *lpaat3-1;lpaat4-2;lpaat5-2* (Supplementary Fig. S7). Therefore, treating the double mutant *lpaat4-2;lpaat5-2* with 10 µM CI976 permitted establishment of primary root growth phenotypic conditions and allowed investigation of the efficiency of protein trafficking.

PA biosynthesis in Arabidopsis roots is only affected in the double mutant treated with CI976

Since disturbing AtLPAAT activities led to a decrease in primary root growth, the amount of neo-synthesized PA in Arabidopsis roots of the WT, the double mutant *lpaat4-2;lpaat5-2*, and the triple mutant *lpaat3-1;lpaat4-2;lpaat5-2* with or without CI976 treatment was quantified. As shown in Fig. 7A (black columns), in the absence of CI976 the amount of neo-synthesized PA in the double mutant *lpaat4-2;lpaat5-2* was reduced to 60% of that of the WT and the triple mutant *lpaat3-1;lpaat4-2;lpaat5-2*. This was correlated only to a weak primary root growth phenotype as mentioned before (Fig. 5). Treatment of the WT and the triple mutant *lpaat3-1;lpaat4-2;lpaat5-2* with 10 µM CI976 (Fig. 7A, red columns) decreased neo-synthesized PA by 60%, reaching a level of neo-synthesized PA similar to that found in the double mutant *lpaat4-2;lpaat5-2* (Fig. 7A, black column). Treating the *lpaat4-2;lpaat5-2* double mutant with 10 µM CI976 (Fig. 7A, red column) led to an additional decrease in PA which reached only ~30–35% of WT and triple mutant *lpaat3-1;lpaat4-2;lpaat5-2* levels (Fig. 7A, black columns). In these conditions, we observed a stronger primary root growth phenotype (Fig. 6). This may indicate a concentration threshold for PA with no clear or very weak phenotype at concentrations above this level and a clear primary root growth phenotype at concentrations below (Fig. 6).

A small decrease in the amount of phospholipids was observed in the double mutant *lpat4-1;lpat5-1* in the study of Angkawijaya *et al.* (2019). Therefore, an additional question was to determine whether the primary root growth phenotype observed in the CI976-treated double mutant *lpaat4-2;lpaat5-2* was only due to a decrease in the neo-synthesis of

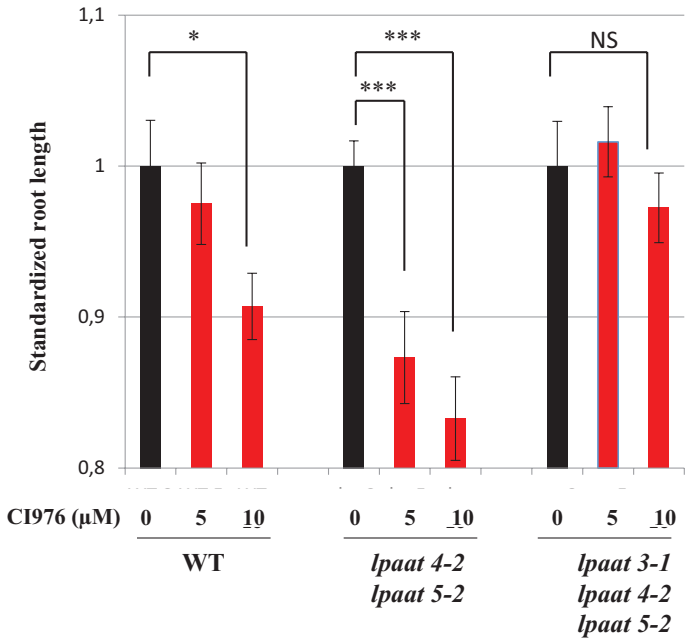

Fig. 6. Sensitivity of the WT, double mutant *lpaat4-2;lpaat5-2*, and triple mutant *lpaat3-1;lpaat4-2;lpaat5-2* lines to CI976 treatment. Seedlings were grown on MS agar medium plates containing different concentrations of CI976 (0, 5, or 10 µM). Primary root length was measured 5 d after germination and standardized to the untreated condition for each line. Data are mean values ±SE from three biological replicates, *n*=60. The asterisks indicate significant difference between untreated conditions (black bar) and CI976-treated conditions (red bars). Statistics were done by non-parametric Kruskal–Wallis rank sum test, ***P<0.001, NS=not significant.

PA or whether the neo-synthesis of the major phospholipids was also affected by the CI976 treatment and could contribute to the primary root growth phenotype. For this, we measured the level of the neo-synthesis of the two major phospholipids PC and PE from [^{14}C]acetate in roots of the WT, the double mutant *lpaat4-2;lpaat5-2*, and the triple mutant *lpaat3-1;lpaat4-2;lpaat5-2* treated with CI976. Beside the significant decrease in labelled PA in the CI976-treated double mutant *lpaat4-2;lpaat5-2* compared with the WT and the triple mutant *lpaat3-1;lpaat4-2;lpaat5-2* (Fig. 7A, red columns), we did not observe any significant decrease in the amounts of labelled PC and PE (Fig. 7B). This indicates that the synthesis capability of these major phospholipids is similar in the CI976-treated double mutant *lpaat4-2;lpaat5-2* compared with the CI976-treated WT and triple mutant *lpaat3-1;lpaat4-2;lpaat5-2*. Therefore, the primary root growth phenotype observed in the CI976-treated double mutant *lpaat4-2;lpaat5-2* (Fig. 6) can be mainly attributed to the disturbance of PA metabolism unrelated to the neo-synthesis of the major phospholipids. By combining genetic and pharmacological approaches, we determined the best conditions, namely the *lpaat4-2;lpaat5-2* double mutant treated with 10 µM CI976, to investigate the potential role of these LPAATs in the functioning of the secretory pathway.

Efficiency of protein secretion in the CI976-treated double mutant lpaat4-2;lpaat5-2

To investigate the efficiency of protein trafficking in the CI976-treated double mutant *lpaat4-2;lpaat5-2*, we decided to look *in situ* at several plasma membrane markers (H^+-ATPases, PIN2, and PIP2,7) with already characterized trafficking to the plasma membrane (Melser *et al.*, 2010; Hachez *et al.*, 2014; Wattelet-Boyer *et al.*, 2016).

We first investigated the trafficking of H^+-ATPases to the plasma membrane using an immunocytochemistry approach. Supplementary Fig. S8 shows that the trafficking to the plasma membrane of H^+-ATPases was not affected in the CI976-treated double mutant *lpaat4-2;lpaat5-2* compared with the WT. As a consequence, the trafficking to the plasma membrane of H^+-ATPases did not seem to require the LPAAT-dependent production of PA.

To investigate the impact of LPAATs on PIN2 trafficking to the plasma membrane, we crossed the stable line pPIN2::PIN2–GFP (Xu and Scheres, 2005) with the WT and the double mutant *lpaat4-2;lpaat5-2* line. Roots were grown with or without 10 µM CI976. Upon CI976 treatment, we observed an increase in intracellular PIN2 in the double mutant (Fig. 8), indicating that the trafficking of PIN2 was disturbed. We also observed that the polarity index of PIN2 was affected, with a value of 2.1 for the double mutant compared with 4.3 for the WT (P<0.001). As a consequence, we also tested the effect on gravitropism but could not find a significant effect. It was shown that in *pin2* mutants, PIN1 is ectopically induced in the PIN2 expression domain in the cortex and epidermis with the same polarity as PIN2, and that some PIN2 localization defects might not necessarily impact gravitropism (Vieten *et al.*, 2005). Therefore, some functional redundancy can act between PIN proteins and could explain our results.

As an approach to try to identify the compartment(s) where PIN2 was retained, we used an immunostaining strategy with antibodies raised against various compartments of the secretory pathway: Echidna (ECH, marker of the SYP61 compartment; Gendre *et al.*, 2011; Boutté *et al.*, 2013), SAR1 (an ERES marker; Hanton *et al.*, 2007), and Membrine11 (Memb11, a *cis*-Golgi marker; Marais *et al.*, 2015). Immunostaining upon CI976 treatment of the double mutant *lpaat4-2;lpaat5-2* expressing PIN2–GFP was performed (Supplementary Fig. S9A–J). A significant co-localization was observed with ECH but not with SAR1 and Memb11 (Supplementary Fig. S9K), indicating that PIN2 was mainly retained at the level of the *trans*-Golgi network (TGN). We also carried out BFA treatment on both CI976-treated WT and *lpaat4-2;lpaat5-2* double mutant plants, and observed the same BFA bodies (Supplementary Fig. S10) with a higher labelling in the case of the double mutant, and without other intracellular structures labelled. This confirmed that PIN2 was effectively present in TGN-derived structures in the *lpaat4-2;lpaat5-2* double mutant treated by BFA.

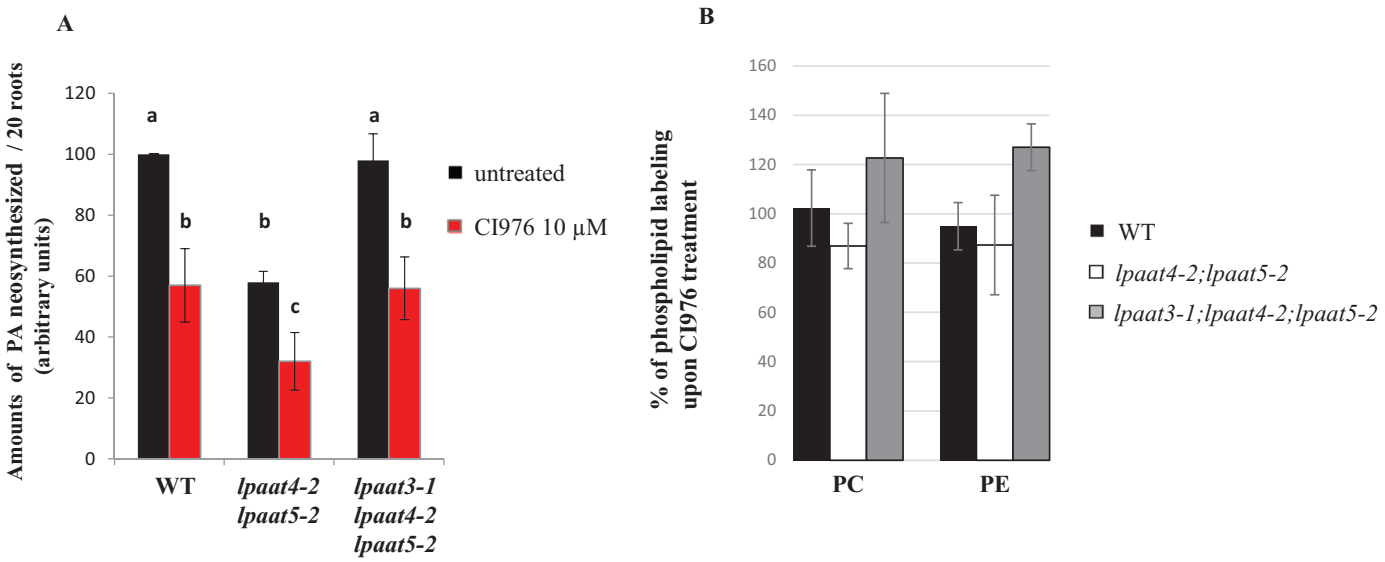

Fig. 7. CI976 treatment affects the neo-synthesis of PA but not that of the major phospholipids in Arabidopsis roots. Seedlings were grown on MS agar medium plates or MS agar medium plates complemented with 10 µM CI976. Primary roots from 20 seedlings were collected 5 d after germination for both conditions and incubated for 4 h with [^{14}C]acetate±10 µM CI976. Lipids were extracted and separated by HPTLC. (A) Amounts of neo-synthesized [^{14}C]PA, [^{14}C]PC, and [^{14}C] PE were quantified for the WT line and the mutant lines *lpaat4-2;lpaat5-2* and *lpaat3-1;lpaat4-2;lpaat5-2*. The amounts of [^{14}C]PA produced were calculated for each line without treatment (black bar) or under treatment (red bar) by taking as 100 the amount of [^{14}C]PA produced in the WT line without treatment. Data are mean values ±SD from three biological replicates. Statistics were carried out using the non-parametric Kruskal–Wallis test; similar letters above bars indicate that datasets are not significantly different, b/a and c/b: P<0.001. (B) [^{14}C]PC and [^{14}C]PE produced were quantified in the WT line, the double mutant line *lpaat4-2;lpaat5-2*, and the triple mutant line *lpaat3-1;lpaat4-2;lpaat5-2* upon CI976 treatment, and compared with the amounts measured for each line without treatment. The percentage of labelling of PC and PE in the presence of CI976 was expressed as compared with the untreated conditions taken as equal to 100. Data are mean values ±SD from three biological replicates. Statistical analysis used the non-parametric Kruskal–Wallis test, and the P-values for PC (0.393) and PE (0.288) show no significant differences.

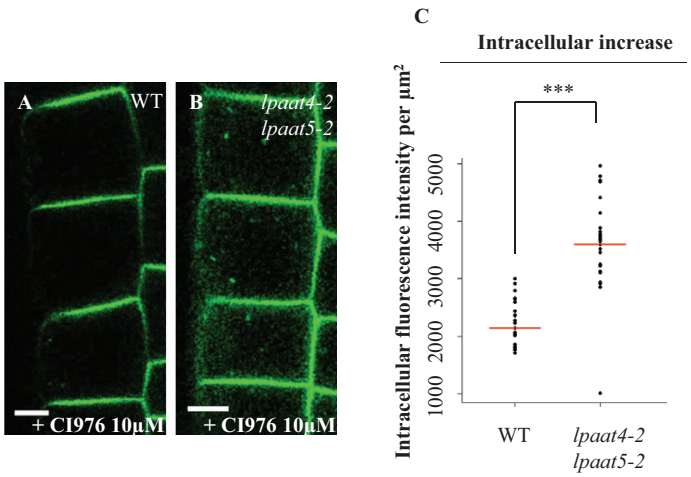

Fig. 8. Auxin carrier PIN2–GFP trafficking is altered in the double mutant *lpaat4-2;lpaat5-2* upon CI976 treatment. Localization of PIN2–GFP in the WT (A) and *lpaat4-2,lpaat5-2* (B) background upon 10 µM CI976 treatment. The sum of fluorescense intensity per µm^2 was calculated in the cytoplasm for each line upon inhibitor treatment. The intracellular increase in PIN2–GFP in *lpaat4-2;lpaat5-2* upon CI976 treatment is shown (C) (n=27 cells quantified over eight independent roots). All the data were represented for each line (black dots) with the median of each dataset (red bar). Statistics were done by non-parametric Kruskal–Wallis rank sum test, ***P<0.001.

To investigate the impact of AtLPAATs on PIP2;7 trafficking to the plasma membrane, the subcellular location of PIP2;7 in the WT, the double mutant *lpaat4-2;lpaat5-2*, and the triple mutant *lpaat3-1;lpaat4-2;lpaat5-2* treated with 10 µM CI976 was analysed. For this, an immunocytochemistry approach to reveal the *in situ* localization of PIP2;7 was used. Whole-mount immunolabelling of Arabidopsis roots was performed as described previously (Boutté and Grebe, 2014). As shown in Fig. 9, a decrease in the mean fluorescence ratio of plasma membrane to cytoplasm was observed for the double mutant *lpaat4-2;lpaat5-2* compared with the WT and the triple mutant *lpaat3-1;lpaat4-2;lpaat5-2* which corresponded to both a decrease in PIP2;7 in the plasma membrane and an increase in the protein amount in the cytoplasm. It was reported that PIP2;7 is highly up-regulated under salt stress (Pou *et al.*, 2016) which also increases *AtLPAAT4* gene transcription in roots (Supplementary Fig. S11). We first checked for sensitivity of the double mutant *lpaat4-2;lpaat5-2* to salt stress. The double mutant *lpaat4-2;lpaat5-2* was effectively more sensitive to salt stress than the WT and the triple mutant *lpaat3-1;lpaat4-2;lpaat5-2* at 50 mM NaCl (Fig. 10). Higher salt concentrations up to 150 mM resulted in stronger phenotypes but without significant differences between the WT plants and the mutant lines. Interestingly, looking at the sensitivity of

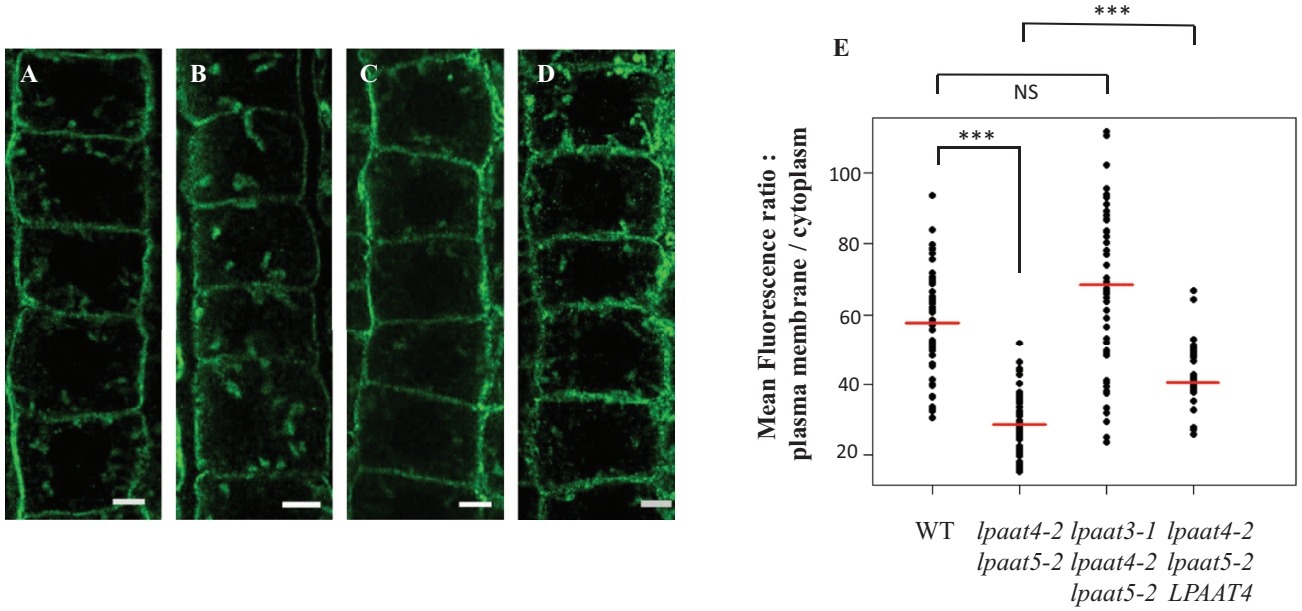

Fig. 9. Aquaporin PIP2;7 trafficking is altered in the double mutant *lpaat4-2;lpaat5-2* upon CI976 treatment. Immunolocalization of the aquaporin PIP2;7 in root epithelial cells from Arabidopsis WT (A), double mutant *lpaat4-2,lpaat5-2* (B), triple mutant *lpaat3-1;lpaat4-2;lpaa5-2* (C), and double mutant *lpaat4-2;lpaat5-2* overexpressing LPAAT4 (D) lines upon CI976 treatment. Scale bar=5 μm. Mean fluorescence intensity was measured at the plasma membrane and in the cytosol for each line upon treatment. The ratio of fluorescence intensity between the plasma membrane and the cytosol was calculated. (E) All the ratios were represented for each line (black dots) with the median of each dataset (red bar). Statistics were done by non-parametric Kruskal–Wallis rank sum test, ***P<0.001; NS, not significant.

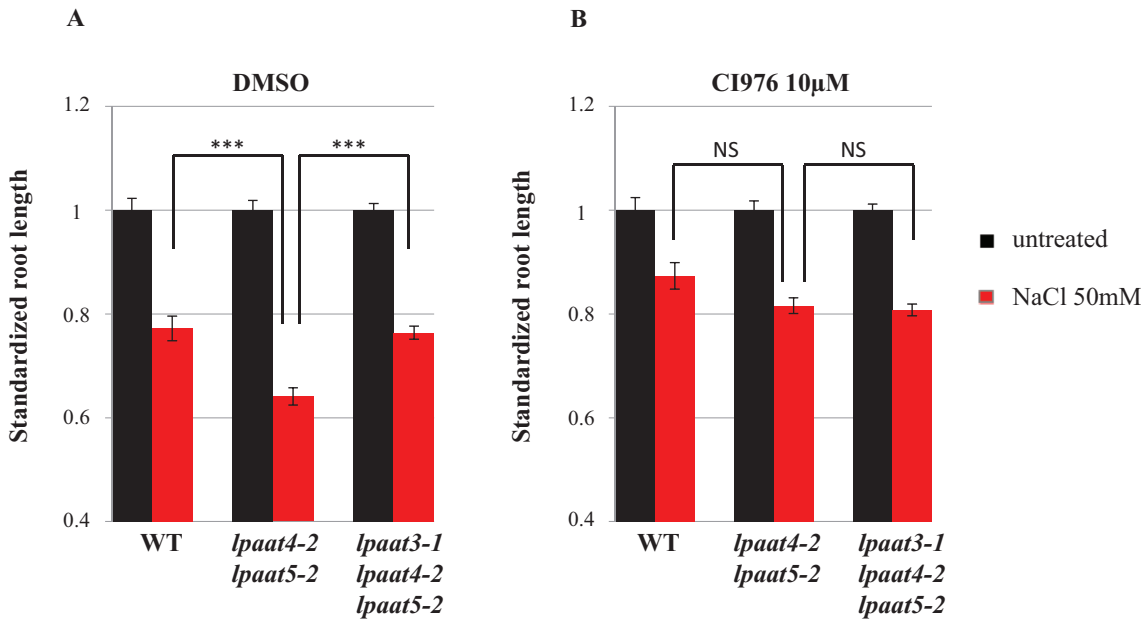

Fig. 10. The double mutant *lpaat4-2;lpaat5-2* is highly sensitive to salt stress as compared with the WT and the triple mutant *lpaat3-1;lpaat4-2;lpaat5-2*. Seedlings were grown on MS agar medium plates supplemented or not with 50 mM NaCl. The same experiment was performed with (A) or without (B) CI976 treatment. Primary root length was measured 5 d after germination. Values were standardized to the WT for each condition. Results indicate a higher sensitivity of the double mutant *lpaat4-2;lpaat5-2* to salt stress in comparison with WT and triple mutant *lpaat3-1;lpaat4-2;lpaat5-2* lines (A), while this sensitivity is lost upon CI976 treatment (B). Data are mean values ±SE from three biological replicates (n=150). Statistics were done by non-parametric Kruskal–Wallis rank sum test, ***P<0.001.

the different lines to salt stress in the presence of CI976 (Fig. 10), we observed that the double mutant *lpaat4-2;lpaat5-2* became less sensitive in the presence of the drug, and reached the value observed in the WT and the triple mutant *lpaat3-1;lpaat4-2;lpaat5-2* (Fig. 10). This is most probably due to less PIP2;7 localizing to the plasma membrane in double mutant *lpaat4-2;lpaat5-2* root cells under CI976 treatment than in the WT and the triple mutant *lpaat3-1;lpaat4-2;lpaat5-2* (Fig. 9). Complementation of the double mutant *lpaat4-2;lpaat5-2* by overexpression of AtLPAAT4 (*AtLPAAT4* relative transcript abundance in the double mutant *lpaat4-2;lpaat5-2* is shown in Supplementary Fig. S12) resulted in a partial restoration of the localization of PIP2;7 at the plasma membrane (Fig. 9). These results, together with the fact that salt stress increases *AtLPAAT4* gene transcription in roots (Pou *et al.*, 2016), suggest that PA formed by some LPAATs is involved in both the correct functionality of the secretory pathway and lipid signalling processes.

The increase in the amounts of PIP2;7 and PIN2 in intracellular membranes was interpreted as a consequence of a decrease in the trafficking of these proteins to the plasma membrane. However, the same result could have been the consequence of an increase in their internalization. To test whether this might have been the case, we measured endocytosis of the marker FM4-64 in both WT and double mutant *lpaat4-2;lpaat5-2* lines treated with CI976. As shown in Supplementary Fig. S13, it was found that the internalization of the marker FM4-64 did not increase but rather was slightly decreased. As a consequence, it is unlikely that the increase of PIP2;7 and PIN2 was due to an increase in endocytosis. Therefore, our results strongly argue that a decrease in the trafficking efficiency of PIP2;7 and PIN2 to the plasma membrane explains the increase of these protein amounts in intracellular compartments.

In addition, our results show that the disruption of the AtLPAAT activities affects to some extent the efficiency of the secretory pathway, followed by PIP2;7 and PIN2 but not H^+-ATPases, suggesting either different sensitivities to PA for their trafficking process or different requirements for it.

Discussion

PA is a central phospholipid metabolic intermediate and essential for the *de novo* synthesis of membrane lipids. It is also a key second messenger and source of other signalling lipids for numerous signalling pathways activated during stress conditions (Pokotylo *et al.*, 2018; Yao and Xue, 2018). PA, like phosphoinositide and phosphatidylserine, is involved in the differentiation of various electrostatic compartments in the cell (Platre *et al.*, 2018) and has been shown to interact more or less specifically with numerous proteins involved in a large variety of cell functions (Pokotylo *et al.*, 2018). PA may also contribute to the function of the plant secretory pathway through its physicochemical properties (Furt and Moreau, 2009; Boutté and Moreau, 2014). From a mechanical point of view, PA is a cone-shaped lipid favouring negative membrane curvature, and its precursor LPA has the tendency to favour positive membrane curvature due to its inverted cone shape. Both of these lipids can stimulate physicochemical mechanisms linked to membrane morphodynamics depending on the membrane leaflet they are produced on (Boutté and Moreau, 2014). Yang *et al.* (2011) have demonstrated the interplay between phospholipase A2 and LPAAT in regulating COPI vesicles versus tubule formation from Golgi membranes in mammalian reconstituted systems. More recently, lysophospholipids have been shown to be critical in the formation of COPII vesicles by inducing the required membrane deformation (Melero *et al.*, 2018). Lysophospholipids are also involved in PIN intracellular trafficking (Lee *et al.*, 2010) as well as pollen germination and development (Kim *et al.*, 2011). In addition to enzymes such as phospholipases which have been shown to be involved in membrane trafficking in plant cells (Li and Xue, 2007; Lee *et al.*, 2010; Kim *et al.*, 2011; Li *et al.*, 2011), acyltransferases which are potentially involved in lipid metabolism in the Land's cycle may have an impact on membrane morphodynamics in plant cells (Boutté and Moreau, 2014).

Interestingly, Pleskot *et al.* (2012) have shown different roles for PA produced by either PLDs or diacylglycerol kinases in pollen tube growth. Their results strongly suggest that several pools of PA may exist according to the biosynthetic pathway followed by PA and the cellular process concerned. Similarly, different LPAATs could produce different pools of PA linked to various cellular processes (*de novo* lipid synthesis for membrane formation, lipid synthesis for stress-related responses, lipid synthesis for mechanical processes in membrane trafficking, etc.). The aim of this study was therefore to investigate the possibility that some LPAATs might have a role in the secretory pathway through PA neo-synthesis not related to the bulk neo-synthesis of membrane phospholipids.

First, we determined that the four extra-plastidial AtLPAAT proteins (AtLPAAT2–AtLPAAT5) are strict LPA acyltransferases which was a prerequisite for such a study. Then, we confirmed that AtLPAAT2, 4, and 5 are ER localized and that they do not cycle between the ER and Golgi bodies. The localization of AtLPAAT3 was unknown, but we showed that AtLPAAT3 is located in round structures corresponding to ERES.

Since AtLPAAT2 is likely to be the primary enzyme for the *de novo* synthesis of PA sustaining the overall *de novo* synthesis of phospholipids in the ER (Angkawijaya *et al.*, 2017), we focused our attention on AtLPAAT3–AtLPAAT5. Given the results obtained on root growth phenotypes with the single, double, and triple mutants, the strategy was to create a combined genetic and biochemical approach as already managed successfully for the study of sphingolipids in the plant secretory pathway (Melser *et al.*, 2010; Wattelet-Boyer *et al.*, 2016).

Treating the double mutant *lpaat4-2;lpaat5-2* with the LPAT inhibitor CI976 (Brown *et al.*, 2008; Schmidt and Brown, 2009; Yang *et al.*, 2011) defined experimental conditions in which a significant decrease in neo-synthesized PA without any decrease in the neo-synthesis of the major phospholipids PC and PE was obtained.

This suggests that under these experimental conditions, other types of LPAT (LPCAT and LPEAT which synthesize new PC and PE from lysophosphatidylcholine and lysophosphatidylethanolamine), that are present in all lines (the double mutant *lpaat4-2;lpaat5-2* as well as the WT and the triple mutant *lpaat3-1;lpaat4-2;lpaat5-2*), are not greatly affected. The effect of the drug was therefore likely to be related to its action on the LPAATs. Since the major phospholipids PC and PE were not decreased, it is likely that the amount of PA synthesized was still sufficient for sustaining phospholipid synthesis but not sufficient for its role related to the trafficking of PIP2;7 and PIN2. Therefore, the effects observed on primary root growth and protein trafficking could probably be attributed to the inhibition of 'specific' pool(s) of PA and that a threshold concentration of PA was required for the trafficking of some proteins.

The fact that PIN2 was partially retained at the TGN but not significantly at the ER ES is intriguing compared with the potential localization of AtLPAAT3. A first possibility could be that some of these AtLPAATs are present in the TGN but at a concentration that was not detected/detectable in our approach. In addition, AtLPAAT3 localization seemed to depend on active ER export motifs, supporting its presence in a post-ER compartment. However, AtLPAAT2–AtLPAAT5 have not so far been identified in Golgi body/TGN proteomes (Drakakaki *et al.*, 2012; Parsons *et al.*, 2012; Groen *et al.*, 2014; Heard *et al.*, 2015). Another possibility would be that ER–TGN connections may support the feeding of PA to the TGN, but no clear relationship has been demonstrated between these two compartments in plant cells as shown in mammalian cells (Mesmin *et al.*, 2017). In addition, Li and Xue (2007) have shown that PA (produced by PLDζ2) is required for the normal cycling of PIN2-containing vesicles and stimulates the gravitropic response. In our conditions, the gravitopic response was not significantly affected. Moreover, Li and Xue (2007) have observed that, in *pld*ζ*2* and PLDζ2-deficient plants, endocytosis in root cells was strongly decreased, leading to smaller BFA compartments. This was probably due to a decrease in the formation of PA at the plasma membrane. In our case, endocytosis was not significantly reduced, and therefore, BFA compartments could still be alimented by both reduced exocytosis at the TGN and endocytosis. Therefore, the effects of PA decrease did not have the same consequences when comparing PLDζ2 -deficient plants and the CI976-treated *lpaat4-2;lpaat5-2* double mutant plants, suggesting that different PA pools are used. Since PIN2 labelling was high in the *lpaat4-2;lpaat5-2* double mutant treated with CI976 and BFA (Supplementary Fig. S10) with similar BFA bodies as compared with the WT, it is likely that the PA decrease through inhibition of ER LPAAT activities resulted in a disturbance of ER–Golgi–TGN trafficking of PIN2 to the plasma membrane, and we do not exclude that PIN2 recycling back to the plasma membrane could also have been affected. As shown in Fig. 9, the potential impact of LPAATs on PIP2;7 trafficking to the plasma membrane was evidenced through both a decrease in PIP2;7 on the plasma membrane and its increase in the cytoplasm. With PIP2;7 being highly regulated under salt stress (Pou *et al.*, 2016) and *AtLPAAT4* gene transcription being enhanced in roots under these conditions (Supplementary Fig. S11), we could perform critical experiments supporting our conclusion that PIP2;7 trafficking to the plasma membrane is linked to LPAAT activities: (i) the double mutant *lpaat4-2;lpaat5-2* was more sensitive to salt stress than the WT and the triple mutant *lpaat3-1;lpaat4-2;lpaat5-2* (Fig. 10); (ii) the double mutant *lpaat4-2;lpaat5-2* became less sensitive to salt stress in the presence of CI976 (Fig. 10); (iii) PIP2;7 localized less to the plasma membrane of double mutant *lpaat4-2;lpaat5-2* root cells under CI976 treatment (Fig. 9); and (iv) complementation of the CI976-treated double mutant *lpaat4-2;lpaat5-2* by overexpression of AtLPAAT4 partially restored the localization of PIP2;7 at the plasma membrane (Fig. 9). Therefore, we were able to correlate the efficiency of PIP2;7 trafficking to the plasma membrane with the functionality of LPAATs. By using a PA-specific optogenetic biosensor which determines the precise spatio-temporal dynamics of PA at the plasma membrane, Li *et al.* (2019) showed that salt stress triggers an accumulation of PA via the activity of a PLDα1. Investigating a *pld*α*1* mutant indicated that PA signalling integrates with cellular pH dynamics to mediate plant responses to salt stress (Li *et al.*, 2019). Therefore, it is likely that PA is involved in both signalling and mechanistic processes in regulating various fundamental biological functions in plants.

Unfortunately, because the immunostaining strategy was not possible with PIP2;7 (primary antibodies being from rabbit like those used for the markers), we could not address the question of the nature of the compartments where PIP2;7 was retained. Hachez *et al.* (2014) found that PIP2;7 interacts with the SNAREs SYP61 and SYP121 to reach the plasma membrane, and we determined that the sorting of PIN2 at the TGN occurs at a SYP61 TGN subdomain (Wattelet-Boyer *et al.*, 2016) where PIN2 was partially retained. We may hypothesize that PIP2;7 was to some extent retained in the same compartment as PIN2. In addition, it has been shown that under salt stress, loss of PLD function impairs auxin redistribution and this resulted in decreased primary root growth (Wang *et al.*, 2019). Therefore, these plasma membrane proteins may have similar dependencies on some aspects of the trafficking machinery, and may also be similarly dependent on a specific formation of PA. Moreover, the data of Wang *et al.* (2019) indicate a role for PA in coupling extracellular salt signalling to PA-regulated PINOID kinase-dependent PIN2 phosphorylation and polar auxin transport. In conclusion, PA produced by different enzymes (PLDs, LPAATs, etc.) at different intracellular sites (early

secretory pathway, late secretory pathway, or plasma membrane) may regulate diverse aspects of protein trafficking, dynamics, and lipid signalling functions. The recent implication of AtLPAAT4 and AtLPAAT5 in nitrogen starvation response (Angkawijaya *et al.*, 2019) also illustrates how the same lipid-metabolizing enzymes can be engaged in multiple different cellular functions (Pokotylo *et al.*, 2018).

Phospholipases and therefore lysophospholipids are involved in membrane trafficking in roots and pollen (Lee *et al.*, 2010; Kim *et al.*, 2011), and AtLPAATs have a role in the trafficking of PIP2;7 and PIN2, and in primary root growth. Hence an interplay between phospholipases and LPAATs is likely to occur in plant cells as already demonstrated in mammalian cells (Yang *et al.*, 2011). Pagliuso *et al.* (2016) identified a key component (CtBP1-S/BARS) of a protein complex that is required for fission of several endomembranes in mammalian cells which binds to and activates a *trans*-Golgi LPAAT protein. This interaction is essential for fission of transport vesicles. Interconversion of LPA and PA probably facilitates the fission process either directly or indirectly [through binding of protein(s) of the machinery to PA]. In addition, the production of PA by PLDs can also be critical for membrane trafficking in plant cells (Pleskot *et al.*, 2012) as evidenced in mammalian cells for vesicle fission (Yang *et al.*, 2011), suggesting that PA produced by different enzymes (PLDs or LPAATs) can be involved at different steps or pathways. We must also consider another potential complexity since some enzymes (cytosolic or membranous) may be active both as a phospholipase (producing lysophospholipids from phospholipids) and as an acyltransferase (to reform a phospholipid) in order to contribute to membrane deformation/re-arrangements involved in the fusion/fission processes via lipid remodelling (Ghosh *et al.*, 2009; Jasieniecka-Gazarkiewicz *et al.*, 2016).

In addition, since the trafficking of H^+-ATPases to the plasma membrane was not affected, this suggests either different sensitivities of the trafficking process of different proteins to PA concentration or different molecular requirements for their trafficking. Such a difference could be related to what has been observed in the role of PA in pollen tube growth (Pleskot *et al.*, 2012). Hence several different mechanisms/pathways need to be considered in the complexity of the regulation of protein trafficking.

Finally, since other lipid families (sterols, sphingolipids, etc.) are also critical in the functioning and regulation of the plant secretory pathway (Laloi *et al.*, 2007; Men *et al.*, 2008; Boutté *et al.*, 2010; Melser *et al.*, 2010; Markham *et al.*, 2011; Wattelet-Boyer *et al.*, 2016), we must consider that a huge interplay between lipids, lipid-synthesizing/modifying enzymes, and lipid-binding proteins is at work to govern and regulate the plant secretory pathway.

In conclusion, we designed an experimental set-up which allowed investigation of the potential involvement of AtLPAATs and PA in the functioning of the plant root secretory pathway. The double mutant *lpaat4-2;lpaat5-2* treated with the LPAT inhibitor CI976 was significantly affected in primary root growth, and the trafficking of PIP2;7 and PIN2 was found to be disturbed. Our results support a critical PA concentration threshold involved in the trafficking of some proteins through the plant root secretory pathway. Since phospholipases and therefore lysophospholipids are involved in protein membrane trafficking in roots (Lee *et al.*, 2010), the implication of AtLPAATs in the trafficking of PIP2;7 and PIN2 in roots also suggests an interplay between phospholipases and LPAATs in root cells as shown in mammalian cells (Yang *et al.*, 2011).

Supplementary data

The following supplementary data are available at *JXB* online.

Table S1. Primers used in the study.

Fig. S1. Characterization of *lpaat* insertion mutant lines and T-DNA positions.

Fig. S2. AtLPAAT3, AtLPAAT4, and AtLPAAT5 expression levels in the different mutant genetic backgrounds.

Fig. S3. Alignment of human LPAAT3 with AtLPAAT2–AtLPAAT5 from Arabidopsis.

Fig. S4. *AtLPAAT3*, *AtLPAAT4*, and *AtLPAAT5* are expressed at similar levels in Arabidospis roots.

Fig. S5. Images of seedlings from the different lines.

Fig. S6. Primary root length of the triple mutant *lpaat3-1;lpaat4-2;lpaat5-2* is stimulated.

Fig. S7. *AtLPAAT2* expression level in primary roots.

Fig. S8. Trafficking of plasma membrane H^+-ATPases is not altered upon CI976 treatment.

Fig. S9. PIN2–GFP accumulates in punctuated structures that co-localize with a TGN marker in the CI976-treated *lpaat4-2;lpaat5-2* double mutant.

Fig. S10. Effect of BFA treatment on CI976-treated seedlings.

Fig. S11. Salt stress (NaCl 150 mM) impact on *LPAAT4* gene expression in roots.

Fig. S12. Expression of *AtLPAAT4* in 5-day-old Arabidopsis roots.

Fig. S13. Endocytosis is not accelerated in the double mutant *lpaat4-2;lpaat5-2* line treated with 10 μM CI976.

Acknowledgements

This work was supported by the CNRS (Centre National de la Recherche Scientifique) and the University of Bordeaux. We thank the Bordeaux Imaging Center, part of the National Infrastructure France-BioImaging supported by the French National Research Agency (ANR-10-INBS-04). Lipidomic analyses were performed on the Bordeaux Metabolome Facility-MetaboHUB (ANR-11-INBS-0010).

Author contributions

VW-B, MLG, YB, J-JB, and PM: conceptualization; VW-B, MLG, FD-D, LM-P, and VK: performing the experiments; VW-B, J-JB, YB, and PM: data

analysis; PM: supervision, and writing the article with contributions of all the authors; PM is the author responsible for contact and ensures communication.

Conflict of interest

The authors declare no conflict of interest.

Data availability

The data supporting the findings of this study are available within the paper and within its supplementary data.

References

Angkawijaya AE, Nguyen VC, Nakamura Y. 2017. Enhanced primary root growth in phosphate-starved Arabidopsis by stimulating de novo phospholipid biosynthesis through the over-expression of LYSOPHOSPHATIDIC ACID ACYLTRANSFERASE 2 (LPAT2). Plant, Cell & Environment **40**, 1807–1818.

Angkawijaya AE, Nguyen VC, Nakamura Y. 2019. LYSOPHOSPHATIDIC ACID ACYLTRANSFERASES 4 and 5 are involved in glycerolipid metabolism and nitrogen starvation response in Arabidopsis. New Phytologist **224**, 336–3511.

Ayciriex S, Le Guédard M, Camougrand N, *et al*. 2012. YPR139c/LOA1 encodes a novel lysophosphatidic acid acyltransferase associated with lipid droplets and involved in TAG homeostasis. Molecular Biology of the Cell **23**, 233–466.

Boutté Y, Frescatada-Rosa M, Men S, *et al*. 2010. Endocytosis restricts Arabidopsis KNOLLE syntaxin to the cell division plane during late cytokinesis. The EMBO Journal **29**, 546–558.

Boutté Y, Grebe M. 2014. Immunocytochemical fluorescent in situ visualization of proteins in Arabidopsis. Methods in Molecular Biology **1062**, 453–472.

Boutté Y, Jonsson K, McFarlane HE, Johnson E, Gendre D, Swarup R, Friml J, Samuels L, Robert S, Bhalerao RP. 2013. ECHIDNA-mediated post-Golgi trafficking of auxin carriers for differential cell elongation. Proceedings of the National Academy of Sciences, USA **110**, 16259–16264.

Boutté Y, Moreau P. 2014. Modulation of endomembranes morphodynamics in the secretory/retrograde pathways depends on lipid diversity. Current Opinion of Plant Biology **22**, 22–29

Brown WJ, Plutner H, Drecktrah D, Judson BL, Balch WE. 2008. The lysophospholipid acyltransferase antagonist CI976 inhibits a late step in COPII vesicle budding. Traffic **9**, 786–797.

Czechowski T, Stitt M, Altmann T, Udvardi MK, Scheible WR. 2005. Genome-wide identification and testing of superior reference genes for transcript normalization in Arabidopsis. Plant Physiology **139**, 5–177.

Drakakaki G, van de Ven W, Pan S, *et al*. 2012. Isolation and proteomic analysis of the SYP61 compartment reveal its role in exocytic trafficking in Arabidopsis. Cell Research **22**, 413–424.

Furt F, Moreau P. 2009. Importance of lipid metabolism for intracellular and mitochondrial membrane fusion/fission processes. International Journal of Biochemistry and Cell Biology **41**, 1828–1836.

Gendre D, Oh J, Boutté Y, *et al*. 2011. Conserved *Arabidopsis* ECHIDNA protein mediates *trans*-Golgi-network trafficking and cell elongation. Proceedings of the National Academy of Sciences, USA **19**, 8048–8053.

Ghosh AK, Chauhan N, Rajakumari S, Daum G, Rajasekharan R. 2009. At4g24160, a soluble acyl-coenzyme A-dependent lysophosphatidic acid acyltransferase. Plant Physiology **151**, 869–881.

Groen AJ, Sancho-Andrés G, Breckels LM, Gatto L, Aniento F, Lilley KS. 2014. Identification of trans-Golgi network proteins in *Arabidopsis thaliana* root tissue. Journal of Proteome Research **13**, 763–776.

Ha KD, Clarke BA, Brown WJ. 2012. Regulation of the Golgi complex by phospholipid remodeling enzymes. Biochimica et Biophysica Acta **1821**, 1078–1088

Hachez C, Laloux T, Reinhardt H, *et al*. 2014. Arabidopsis SNAREs SYP61 and SYP121 coordinate the trafficking of plasma membrane aquaporin PIP2;7 to modulate the cell membrane water permeability. The Plant Cell **26**, 3132–3147.

Hanton SL, Chatre L, Renna L, Matheson LA, Brandizzi F. 2007. De novo formation of plant endoplasmic reticulum export sites is membrane cargo induced and signal mediated. Plant Physiology **143**, 1640–1650.

Heard W, Sklenář J, Tomé DF, Robatzek S, Jones AM. 2015. Identification of regulatory and cargo proteins of endosomal and secretory pathways in *Arabidopsis thaliana* by proteomic dissection. Molecular Cell Proteomics **14**, 1796–1813

Jasieniecka-Gazarkiewicz K, Demski K, Lager I, Stymne S, Banaś A. 2016. Possible role of different yeast and plant lysophospholipid:acyl-CoA acyltransferases (LPLATs) in acyl remodelling of phospholipids. Lipids **51**, 15–23.

Kim HU, Huang AH. 2004. Plastid lysophosphatidyl acyltransferase is essential for embryo development in Arabidopsis. Plant Physiology **134**, 1206–1216.

Kim HU, Li Y, Huang AHC. 2005. Ubiquitous and endoplasmic reticulum-located lysophosphatidyl acyltransferase, LPAT2, is essential for female but not male gametophyte development in Arabidopsis. The Plant Cell **17**, 1073–1089.

Kim HJ, Ok SH, Bahn SC, Jang J, Oh SA, Park SK, Twell D, Ryu SB, Shin JS. 2011. Endoplasmic reticulum- and Golgi-localized phospholipase A2 plays critical roles in Arabidopsis pollen development and germination. The Plant Cell **23**, 94–110.

Körbes AP, Kulcheski FR, Margis R, Margis-Pinheiro M, Turchetto-Zolet AC. 2016. Molecular evolution of the lysophosphatidic acid acyltransferase (LPAAT) gene family. Molecular Phylogenetics and Evolution **96**, 55–69.

Laloi M, Perret AM, Chatre L, *et al*. 2007. Insights into the role of specific lipids in the formation and delivery of lipid microdomains to the plasma membrane of plant cells. Plant Physiology **143**, 461–472.

Lee OR, Kim SJ, Kim HJ, Hong JK, Ryu SB, Lee SH, Ganguly A, Cho HT. 2010. Phospholipase A_2 is required for PIN-FORMED protein trafficking to the plasma membrane in the Arabidopsis root. The Plant Cell **22**, 1812–1825.

Lewin TM, Wang P, Coleman RA. 1999. Analysis of amino acid motifs diagnostic for the sn-glycerol-3-phosphate acyltransferase reaction. Biochemistry **38**, 5764–5771.

Li M, Bahn SC, Guo L, Musgrave W, Berg H, Welti R, Wang X. 2011. Patatin-related phospholipase pPLAIIIβ-induced changes in lipid metabolism alter cellulose content and cell elongation in Arabidopsis. The Plant Cell **23**, 1107–1123.

Li W, Song T, Wallrad L, Kudla J, Wang X, Zhang W. 2019. Tissue-specific accumulation of pH-sensing phosphatidic acid determines plant stress tolerance. Nature Plants **5**, 1012–1021.

Li G, Xue HW. 2007. Arabidopsis PLDζ2 regulates vesicle trafficking and is required for auxin response. The Plant Cell **19**, 281–295.

Marais C, Boyer-Wattelet V, Bouyssou G, Hocquellet A, Dupuy JW, Batailler B, Brocard L, Boutté Y, Maneta-Peyret L, Moreau P. 2015. The Qb-SNARE Memb11 interacts specifically with Arf1 in the Golgi apparatus of *Arabidopsis thaliana*. Journal of Experimental Botany **66**, 6665–6678

Markham JE, Molino D, Gissot L, Bellec Y, Hématy K, Marion J, Belcram K, Palauqui JC, Satiat-Jeunemaître B, Faure JD. 2011. Sphingolipids containing very-long-chain fatty acids define a secretory pathway for specific polar plasma membrane protein targeting in Arabidopsis. The Plant Cell **23**, 2362–2378.

Melero A, Chiaruttini N, Karashima T, Riezman I, Funato K, Barlowe C, Riezman H, Roux A. 2018. Lysophospholipids facilitate COPII vesicle formation. Current Biology **28**, 1950–1958.

Melser S, Batailler B, Peypelut M, Poujol C, Bellec Y, Wattelet-Boyer V, Maneta-Peyret L, Faure JD, Moreau P. 2010. Glucosylceramide biosynthesis is involved in Golgi morphology and protein secretion in plant cells. Traffic **11**, 479–490.

Melser S, Molino D, Batailler B, Peypelut M, Laloi M, Wattelet-Boyer V, Bellec Y, Faure JD, Moreau P. 2011. Links between lipid homeostasis, organelle morphodynamics and protein trafficking in eukaryotic and plant secretory pathways. Plant Cell Reports **30**, 177–193.

Men S, Boutté Y, Ikeda Y, Li X, Palme K, Stierhof YD, Hartmann MA, Moritz T, Grebe M. 2008. Sterol-dependent endocytosis mediates post-cytokinetic acquisition of PIN2 auxin efflux carrier polarity. Nature Cell Biology **10**, 237–244.

Mesmin B, Bigay J, Polidori J, Jamecna D, Lacas-Gervais S, Antonny B. 2017. Sterol transfer, PI4P consumption, and control of membrane lipid order by endogenous OSBP. The EMBO Journal **36**, 3156–3174.

Miroux B, Walker JE. 1996. Over-production of proteins in *Escherichia coli*: mutant hosts that allow synthesis of some membrane proteins and globular proteins at high levels. Journal of Molecular Biology **260**, 289–298.

Pagliuso A, Valente C, Giordano LL, *et al*. 2016. Golgi membrane fission requires the CtBP1-S/BARS-induced activation of lysophosphatidic acid acyltransferase δ. Nature Communications **7**, 12148

Parsons HT, Christiansen K, Knierim B, *et al*. 2012. Isolation and proteomic characterization of the Arabidopsis Golgi defines functional and novel components involved in plant cell wall biosynthesis. Plant Physiology **159**, 12–26.

Pascal S, Bernard A, Sorel M, Pervent M, Vile D, Haslam RP, Napier JA, Lessire R, Domergue F, Joubès J. 2013. The *Arabidopsis Cer26* mutant, like the *Cer2* mutant, is specifically affected in the very long chain fatty acid elongation process. The Plant Journal **73**, 733–746.

Platre MP, Noack LC, Doumane M, *et al*. 2018. A combinatorial lipid code shapes the electrostatic landscape of plant endomembranes. Developmental Cell **45**, 465-480

Pleskot R, Pejchar P, Bezvoda R, Lichtscheidl IK, Wolters-Arts M, Marc J, Zárský V, Potocký M. 2012. Turnover of phosphatidic acid through distinct signaling pathways affects multiple aspects of pollen tube growth in tobacco. Frontiers in Plant Science **3**, 54.

Pokotylo I, Kravets V, Martinec J, Ruelland E. 2018. The phosphatidic acid paradox: too many actions for one molecule class? Lessons from plants. Progress in Lipid Research **71**, 43–53.

Pou A, Jeanguenin L, Milhiet T, Batoko H, Chaumont F, Hachez C. 2016. Salinity-mediated transcriptional and post-translational regulation of the Arabidopsis aquaporin PIP2;7. Plant Molecular Biology **92**, 731–744.

Schmidt JA, Brown WJ. 2009. Lysophosphatidic acid acyltransferase 3 regulates Golgi complex structure and function. Journal of Cell Biology **186**, 211–218.

Sparkes IA, Runions J, Kearns A, Hawes C. 2006. Rapid, transient expression of fluorescent fusion proteins in tobacco plants and generation of stably transformed plants. Nature Protocols **1**, 2019–2025.

Testet E, Laroche-Traineau J, Noubhani A, Coulon D, Bunoust O, Camougrand N, Manon S, Lessire R, Bessoule JJ. 2005. Ypr140wp, 'the yeast tafazzin', displays a mitochondrial lysophosphatidylcholine (lyso-PC) acyltransferase activity related to triacylglycerol and mitochondrial lipid synthesis. The Biochemical Journal **387**, 617–626.

Vieten A, Vanneste S, Wisniewska J, Benková E, Benjamins R, Beeckman T, Luschnig C, Friml J. 2005. Functional redundancy of PIN proteins is accompanied by auxin-dependent cross-regulation of PIN expression. Development **132**, 4521–4531.

Wang P, Shen L, Guo J, Jing W, Qu Y, Li W, Bi R, Xuan W, Zhang Q, Zhang W. 2019. Phosphatidic acid directly regulates pinoid-dependent phosphorylation and activation of the PIN-FORMED2 auxin efflux transporter in response to salt stress. The Plant Cell **31**, 250–271.

Wang P, Wang Z, Dou Y, Zhang X, Wang M, Tian X. 2013. Genome-wide identification and analysis of membrane-bound O-acyltransferase (MBOAT) gene family in plants. Planta **238**, 907–922

Wattelet-Boyer V, Brocard B, Jonsson K, *et al*. 2016. Enrichment of hydroxylated C24- and C26-acyl-chain sphingolipids mediates PIN2 apical sorting at trans-Golgi network subdomains. Nature Communications **7**, 12788.

Xu J, Scheres B. 2005. Dissection of Arabidopsis ADP-RIBOSYLATION FACTOR 1 function in epidermal cell polarity. The Plant Cell **17**, 525–536.

Yang JS, Gas H, Lee SY, *et al*. 2008. A role for phosphatidic acid in COPI vesicle fission yields insights into Golgi maintenance. Nature Cell Biology **10**, 1146–1153.

Yang JS, Valente C, Polishchuk RS, *et al*. 2011. COPI acts in both vesicular and tubular transport. Nature Cell Biology **13**, 996–1003.

Yao HY, Xue HW. 2018. Phosphatidic acid plays key roles in regulating plant development and stress responses. Journal of Integrative Plant Biology **60**, 851–863.

Yu B, Wakao S, Fan J, Benning C. 2004. Loss of plastidic lysophosphatidic acid acyltransferase causes embryo-lethality in *Arabidopsis*. Plant & Cell Physiology **45**, 503–510.